Material and Energy Flows in the Production of Cathode and Anode Materials for Lithium Ion Batteries

Energy Systems Division

Material and Energy Flows in the Production of Cathode and Anode Materials for Lithium Ion Batteries

by
Jennifer B. Dunn,[1] Christine James,[2] Linda Gaines,[1] Kevin Gallagher,[3] Qiang Dai,[1] Jarod C. Kelly[1]

[1] Energy Systems Division, Argonne National Laboratory

[2] Chemical Engineering and Materials Science Department, Michigan State University

[3] Chemical Sciences and Engineering Division, Argonne National Laboratory

September 2015

CONTENTS

FIGURES

TABLES

ABSTRACT

The Greenhouse gases, Regulated Emissions and Energy use in Transportation (GREET) model has been expanded to include four new cathode materials that can be used in the analysis of battery-powered vehicles: lithium nickel cobalt manganese oxide ($LiNi_{0.4}Co_{0.2}Mn_{0.4}O_2$ [NMC]), lithium iron phosphate ($LiFePO_4$ [LFP]), lithium cobalt oxide ($LiCoO_2$ [LCO]), and an advanced lithium cathode ($0.5Li_2MnO_3 \cdot 0.5LiNi_{0.44}Co_{0.25}Mn_{0.31}O_2$ [LMR-NMC]). In GREET, these cathode materials are incorporated into batteries with graphite anodes. In the case of the LMR-NMC cathode, the anode is either graphite or a graphite-silicon blend. Lithium metal is also an emerging anode material. This report documents the material and energy flows of producing each of these cathode and anode materials from raw material extraction through the preparation stage. For some cathode materials, we considered solid state and hydrothermal preparation methods. Further, we used Argonne National Laboratory's Battery Performance and Cost (BatPaC) model to determine battery composition (e.g., masses of cathode, anode, electrolyte, housing materials) when different cathode materials were used in the battery. Our analysis concluded that cobalt- and nickel-containing compounds are the most energy intensive to produce.

1 INTRODUCTION

Lithium-ion batteries can incorporate several different types of cathode materials. Lithium cobalt oxide ($LiCoO_2$, or LCO), a layered transition metal oxide, is the most common cathode material, particularly for use in consumer electronic applications. Alternatives to this cathode material are sought to either eliminate or reduce cobalt in cathode materials because of its high cost and limited availability. In addition, LCO has limited stability compared to other cathode materials and can exhibit a decline in performance during recharging (Fergus 2010). Adding nickel, which costs less and has a higher capacity than cobalt, to the layered cathode material can increase stability during delithiation, which occurs during charging, and improve cycling performance. Lithium manganese oxide ($LiMn_2O_4$, or LMO) is also considered a promising cathode material and is a primary constituent in the cathodes of commercial hybrid electric vehicle (HEV), plug-in HEV (PHEV), and EV batteries. Unlike layered metal oxide cathode materials that have a planar structure, LMO has a spinel structure, which creates three-dimensional routes for lithiation and delithiation. LMO is significantly less expensive than cobalt-containing cathode materials because of the high manganese content. An important disadvantage of LMO is its lower capacity compared to layered transition metal oxide cathode materials with cobalt and/or nickel. LMO also suffers from accelerated full cell decay when exposed to the elevated temperatures that commonly occur during operation. Lithium iron phosphate ($LiFePO_4$, or LFP), with an olivine structure, has become another popular material owing to its great thermal stability. LFP, however, has low conductivity that is generally improved with a carbon coating. As with LMO, the energy density of LFP is lower than traditional layered metal oxide cathode materials; however, LFP and LMO are both less expensive on a mass basis than the layered materials.

Figure 1 outlines the processes involved in battery production and assembly, or the cradle-to-gate portion of a battery's life cycle. The choice of materials used in the battery, including the choice of cathode material, affects the energy consumed and air pollutants, including greenhouse gases (GHGs), emitted from cradle-to-gate. In earlier research, we developed detailed material and energy flow data for the production of LMO (Dunn et al. 2014). These data were incorporated into the vehicle cycle module of Argonne National Laboratory's (Argonne's) Greenhouse gases, Regulated Emissions and Energy use in Transportation (GREET2) model and analyzed to identify the key contributors to LMO battery production and assembly (Dunn et al. 2012b). One other environmental analysis of lithium-ion batteries considered LMO as the cathode (Notter et al. 2010). Another examined nickel metal hydride, NMC, and LFP (Majeau-Bettez et al. 2011) as the cathode materials. Other recent reports focused on NMC cathode materials (Ellingsen et al. 2014) and silicon nanowires as the anode with NMC as the cathode (Li et al. 2014). Prior to the present analysis, only LMO was included as a cathode material in GREET.

Materials Acquisition	Materials Transportation and Distribution	Battery Assembly
• Recovery: metals and ore mining, crude oil recovery • Processing: metals beneficiation, production of structural materials including steel, plastics, aluminum	• Transportation of raw materials to point of processing • Transportation of battery assembly inputs to plant	• Electrode materials preparation • Electrode coating • Calendaring • Electrode slitting • Electrolyte filling and cell closing • Formation cycling • Module assembly • Battery assembly

Figure 1 Battery Cradle-to-Gate Diagram with Examples of Processes in Each Phase

This report (Section 2) develops material and energy flows for the following cathode materials: LCO, LFP, lithium nickel cobalt manganese oxide ($LiNi_{0.4}Co_{0.2}Mn_{0.4}O_2$, or NMC), and the lithium and manganese-rich metal oxide $0.5Li_2MnO_3\cdot0.5LiNi_{0.44}Co_{0.25}Mn_{0.31}O_2$ (LMR-NMC). The latter cathode material is under development at Argonne National Laboratory. LMR-NMC was included in this study because it is a promising material with high energy density and low cost. The main drawback to this material, however, is that it degrades quickly. NMC, LFP, and LCO were all chosen because they are commonly used and are reasonably successful (Fergus 2010). Table 1 outlines the capacity, advantages, and drawbacks of the different cathodes for which material and energy flows are developed in this report, as well as for lithium manganese oxide (LMO). The anode materials included in GREET are graphite and silicon. In GREET, silicon is only used in combination with graphite for batteries with an LMR-NMC cathode material.

It is important to emphasize that the material and energy flows developed in this report are subject to large uncertainties. First, the preparation techniques for some of these cathode materials (e.g., LMR-NMC) are either under development or are not at commercial scale. Second, even for cathode materials produced at commercial scale (i.e., LCO), publicly available data on the energy and materials consumed in their preparation are scarce. In our analysis, we rely on public information in patents and journal articles to develop material and energy flows. Results should therefore be interpreted as an estimate of the energy and environmental intensity of preparing these cathodes. Because they were developed with a consistent methodology, the estimates can be cross-compared to assess which cathode materials are likely to be more energy- and emissions-intensive to produce. In addition, the analysis can be used to identify the most intensive steps in the production of any one cathode material and subsequently help guide research and development decisions to minimize energy consumption and environmental impacts. Moreover, cathode developers can populate GREET with cathode-specific data to assess the supply chain of the cathodes they are examining.

The amounts of cathode material, anode material, electrolyte, and structural materials used in batteries for hybrid electric vehicles (HEVs), plug-in HEVs (PHEV), and battery electric vehicles (BEVs) are determined by modeling the batteries with Argonne National Laboratory's Battery Performance and Cost (BatPaC) model (Nelson et al. 2011). We describe this modeling in Section 3 of this report. Appendix A contains BatPaC results for different vehicle types (HEVs, PHEVs, BEVs) with different cathode materials.

After the battery use phase, which can be modeled with the fuel cycle model of GREET (GREET 1), the battery could be disposed or recycled. An additional option for end-of-life is battery repurposing as an energy storage device (Neubauer and Pesaran 2010). In our previous work (Dunn et al. 2014), we developed material and energy flow data for three battery recycling technologies, a pyrometallurgical process that recovers LCO, an intermediate process that recovers cobalt and Li_2CO_3 separately, and a direct process that recovers LCO and requires some relithiation of the cathode material. GREET as released in July 2012 contained data for recycling of LCO cathode batteries with the pyrometallurgical process. Now it has been expanded to consider intermediate and direct recycling for NMC, LMR-NMC, LCO, and LFP. As noted in earlier publications, the material and energy flow data we developed for battery recycling technologies is subject to significant uncertainty because these technologies are still emerging, and public information concerning their energy and material intensity is limited.

Table 1   Cathode Material Properties (BatPaC)

Chemical Formula	Abbreviation	Specific Energy (Wh/kg vs. Li-metal)	Capacity (mA/g)	Advantage(s)	Drawback(s)
$LiMn_2O_4$	LMO	405	100	• Low cost • High power density	• Lower energy density • Accelerated capacity fade
$LiCoO_2$	LCO	610	150	• High energy density	• High cost • Moderate stability
$LiFePO_4$	LFP	515	150	• High power density • Very stable	• Lower energy density
$LiNi_{0.4}Co_{0.2}Mn_{0.4}O_2$	NMC	675	150	• Performs well for all metrics	• Moderate cost • Moderate stability
$0.5Li_2MnO_3$ $0.5LiNi_{0.44}Co_{0.25}Mn_{0.31}O_2$	LMR-NMC	940	250	• High energy density • Low cost	• Not commercial • Degrades quickly

2 ENERGY INTENSITY OF ELECTRODE MATERIAL
AND PRECURSOR PRODUCTION

In this section, we describe in detail the production of four cathode materials: NMC (2.1), LFP (2.2), LCO (2.3), and LMR-NMC (2.4). In addition, we document data sources used in the development of the silicon data in GREET (2.5). Each subsection contains a diagram of the production of each cathode material. The final step in this supply chain is the preparation of the cathode material. For LCO and LFP, we considered two types of preparation, hydrothermal (HT) and solid state (SS). When necessary, we develop material and energy flow data for compounds that were not included in GREET as released in July 2012. We note that the energy values in this report are purchased energy, or the energy consumed at the facility that is producing each compound in the supply chain, and are reported as lower heating values (LHVs). When these purchased energy data are incorporated in GREET, the full fuel cycle energy is calculated based on GREET parameters for the energy consumed in the provision of energy to the point of use. For example, GREET calculates that approximately 1.1 million Btu (mmBtu) are consumed to provide 1 mmBtu of natural gas. The analysis of cathode materials uses some pre-existing GREET data for the following cathode material precursors: lithium hydroxide (Dunn et al. 2014), sodium hydroxide (Dunn et al. 2012a), nickel oxide (Burnham et al. 2006), cobalt oxide (Burnham et al. 2006), manganese carbonate ore (Burnham et al. 2006), ammonia (Johnson et al. 2013), phosphoric acid (H_3PO_4) (Johnson et al. 2013), lithium carbonate (Li_2CO_3) (Dunn et al. 2014), diammonium phosphate (Johnson et al. 2013), hydrochloric acid (Dunn et al. 2014), and graphite (Dunn et al. 2014). It is important to note that the energy and material flow data we generate in the following subsections simplify the processes to produce cathodes and their precursors and therefore should be regarded as estimates based on engineering calculations. We exclude steps that would occur in actual facilities such as transport of materials around facilities and waste and air emissions treatment and treat heat integration simply. Should data become available to improve these estimates, the estimates in GREET will be revised along with this technical report.

2.1 Material and Energy Flows in the Preparation of NMC

Figure 2 depicts the production of NMC from the production of metal sulfates to the final preparation of the cathode material by a solid state synthesis method. The following subsections provide data underpinning GREET parameters for each of these steps.
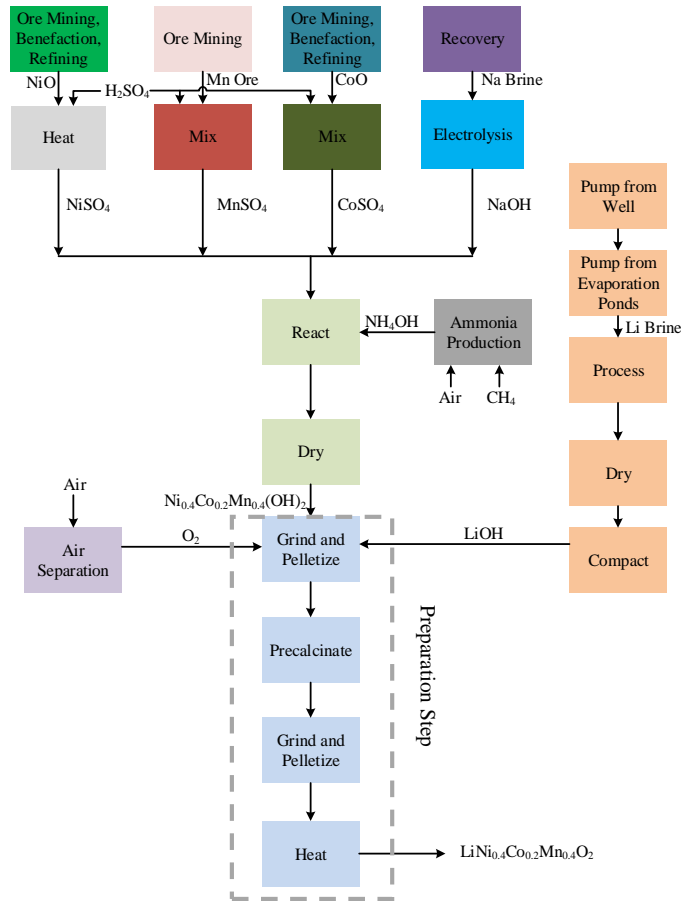
Figure 2 Production of NMC (Note that co-products such as Cl₂ production from sodium brine electrolysis are not shown. Co-product allocation is handled within GREET as described in this report or earlier reports as cited herein.)

2.1.1   Production of Metal Sulfates

Three metal sulfates are used in the preparation of NMC: nickel sulfate, manganese sulfate, and cobalt sulfate. Production of each of the sulfates begins with mining of the metal.

Two types of nickel ore are mined and generally purified for example by electrolytic refining (Tundermann et al. 2013). One type is sulfide ore, which historically has been the dominant nickel source. The second ore type is called laterite and production from this ore is increasing (Mudd 2009). In the case of sulfide ore, nickel is in a physical mixture with iron and copper. These distinct metals can be concentrated by mechanical techniques like flotation (Tundermann et al. 2013). After these physical techniques, sulfide ores undergo pyrometallurgical processes such as smelting and roasting. After these steps and additional, high-temperature purification steps, the resulting nickel sulfide is either cast into anodes to facilitate electrolysis in the production of high-purity nickel or roasted to produce a nickel oxide sinter.

Separation of nickel from laterite ores, on the other hand, requires chemical techniques to extract nickel. One option involves pyrometallurgical processes that produce a nickel matte. The oxide can be produced from roasting the nickel matte. Hydrometallurgical processes leach the ore with ammonia or sulfuric acid. In the latter case, nickel enters solution, which is then purified and produces nickel sulfides, which can be converted to a sulfate solution.

Several techniques are possible to produce nickel sulfate solutions including the above. Because the data for nickel currently in GREET is for nickel oxide, we adopted a pathway to nickel sulfate in which nickel oxide is mixed and reacts with sulfuric acid (dilute aqueous solution, assumed to be 9.82 wt%) at 49°C (Antonsen and Meshri 2005). We assume that the heat of mixing and reaction are negligible. The energy consumed in producing $NiSO_4$ is then the energy associated with heating the reactants, which are the H_2SO_4 solution and the NiO. We adopt a heat capacity (C$_P$) of 3.84 $\frac{J}{g\ °C}$ for the 9.92 wt% solution of H_2SO_4 (Perry and Green 1997). The C$_P$ of the NiO is the average of its value at 25°C and 49°C as calculated with Equation 1 (Perry and Green 1997).

$$C_{P,NiO} = 11.3 + 0.00215T \qquad [1]$$

where T is the temperature (K) at which the C$_p$ is being calculated.

In future research, we will consider differences in the production of nickel (and associated cobalt) from different types of ores and purification processes.

We used Equation 2 to calculate the energy consumed in heating both the H_2SO_4 solution and the NiO without considering any mixing effects. We assumed that a natural gas boiler provides the requisite energy for $NiSO_4$ production with an efficiency rate of 80%. As a result, the input value for energy consumption of $NiSO_4$ production in GREET is 0.66 mmBtu/ton $NiSO_4$. The amount of H_2SO_4 and NiO consumed in the reaction is based on stoichiometry.

$$q_s = C_P \cdot \Delta T \qquad [2]$$

Cobalt can be recovered in oxide, pure metal, or, in some cases, sulfate form, although the process to produce the sulfate suffers from inefficiencies and severe operating conditions (Hodge et al. 2010). Without specific information on the production of battery-grade $CoSO_4$, we model its production from the reaction of the metal oxide (CoO) and H_2SO_4 (Richardson 2003). Similarly, $MnSO_4$ is assumed to be produced from the combination of a mining product (MnO) and H_2SO_4 in a simple mixing step (Pisarczyk 2005) that does not require heat input. For the preparation of Co and Mn sulfates, we again assumed that the heat of reaction is negligible. As a result, the energy and environmental burdens associated with the two sulfates are those from the production of the raw materials, which we assumed are consumed in stoichiometric amounts. Existing GREET data for CoO, MnO, and H_2SO_4 (Burnham et al. 2006) were used. It is important to note that the metal sulfates here may require additional processing, such as electrolytic processes, which we did not consider, to achieve a battery-grade metal purity. Further investigation of the supply chain of cathode metals Co and Ni will be a topic of future research.

2.1.2 Preparation of $Ni_{0.4}Co0.2Mn_{0.4}(OH)_2$ Precursor

The calculations for $Ni_{0.4}Co_{0.2}Mn_{0.4}(OH)_2$ were based on a procedure to produce $Ni_{1/3}Co_{1/3}Mn_{1/3}(OH)_2$ in a continuously stirred tank reactor (CSTR) at 60°C as proposed by Lee et al. (2004). The metal sulfate solutions are added at a concentration of 2/3 mol/L. NaOH is added to the solution in a stoichiometric amount. We adopted the mid-range value of NH_4OH consumed—0.24 mol/L—as reported in Lee et al. (2004).

We adopted the methodology of Majeau-Bettez et al. (2011) to calculate the total purchased energy (q_t) for the preparation of this precursor as the sum of the heat used in the reactor (q_{CSTR}), the energy required for stirring the CSTR (q_{stir}), and the energy required to heat the solution ($q_{solvent}$) as outlined in Equations 3–5. We also included the energy required to dry the product. The sum of the energy required to heat the solvent and dry the product is halved because we assume that half of this heat can be recovered and re-used in the process through heat integration.

$$q_{t,NCMOH} = q_{CSTR} + q_{stir} + \frac{q_{solvent}}{2} + q_{dry} \qquad [3]$$

where:

$q_{t,NMCOH}$ is the total purchased energy consumed in the preparation of
   $Ni_{0.4}Co_{0.2}Mn_{0.4}(OH)_2$;
q_{CSTR} is the energy consumed in heating the reactor;
q_{stir} is the energy consumed in stirring the reactor; and
q_{dry} is the energy consumed in drying the product.

$$\boldsymbol{q_{CSTR}} = \frac{\lambda A(T_r\text{-}T_0)t_r}{x} \qquad [4]$$

where:

λ is the thermal conductivity of the insulation ($0.04\ \boldsymbol{\frac{W}{m \cdot K}}$);
x is the thickness of the insulation (0.1 m);
A is the surface area of the reactor (25 m^2);
T_0 is the reactor wall temperature (25°C);
T_r is the temperature of the reactor (60°C); and
t_r is the reaction time (12 hours).

The solvent must be heated from 25°C to 60°C. The purchased energy consumed in this step is calculated with Equation 5, in which we make the simplifying assumption that the solution is mostly water. Heating the solvent consumes natural gas combusted in an 80% efficient boiler.

$$q_s = \Sigma C_p \, \Delta T + \Delta H_{vap} \qquad [5]$$

where:

C_p is the average heat capacity of water between 25°C and 60°C;
ΔT is the change in temperature for the drying step; and
ΔH_{vap} is the heat of vaporization of water (3.05 MJ/kg H_2O), added only if water is heated above its boiling point.

The energy consumed in that step to heat the water is also calculated with Equation 5. We again assume that half of the heat used in the drying step can be recovered. The total process energy is calculated with Equation 3.

The energy (electricity) consumed in stirring (20.92 MJ/hr) is based on a CSTR in a process design report (Humbird et al. 2011).

When all contributors to purchased energy consumption in the preparation of this precursor are combined, the result is 8.8 mmBtu/ton $Ni_{0.4}Co_{0.2}Mn_{0.4}(OH)_2$ produced. A total of 99% of the consumed energy is in the form of natural gas; the balance is electricity.

2.1.3 Solid-State Preparation of NMC

Calculation of the energy consumed in the solid state preparation of NMC is based upon the work of Majeau-Bettez et al. (2011) (Figure 2). In this process, solid lithium hydroxide (LiOH) is mixed with $Ni_{0.4}Co_{0.2}Mn_{0.4}(OH)_2$. The mixture is ground and pelletized, precalcinated, reground, repelletized, and then heated to form $LiNi_{0.4}Co_{0.2}Mn_{0.4}O_2$, which is one of the cathode materials.

The energy consumed in the process includes the energy expended to heat both the reactor and the reactants as in Equation 6. In the absence of sufficient physical property data to calculate the heat of the reaction, we neglect it.

$$q_{total,NCM} = q_{oven} + q_{reactants} \qquad [6]$$

where:

$q_{total,NMC}$ = the total purchased energy consumed in the preparation of NMC;
q_{oven} = purchased energy consumed in heating the oven; and
$q_{reactants}$ = purchased energy consumed in heating the reactants.

$q_{reactants}$ for each step was calculated with Equation 7. The mixture was heated from room temperature to 450°C and then from room temperature to 800°C.

$$q_{reactants} = C_P \Delta T \qquad [7]$$

where:

C_p is the heat capacity of the solid reactants [1.05 J/g°C] (Perry and Green 1997); and ΔT is the change in temperature.

The energy required to heat the oven, q_{oven}, was calculated with Equation 8, assuming that 0.55 kg of $LiNi_{0.4}Co_{0.2}Mn_{0.4}O_2$ was produced per liter of input (Majeau-Bettez et al. 2011). Key assumptions in its calculation, based on Majeau-Bettez et al. (2011), were that the chamber furnace has a volume of 8,300 L and is 33% efficient. Furthermore, the precalcination step was assumed to be at 450°C, requiring 12.5 kW for 12 hours, whereas the heating step was assumed to be at 800°C, requiring 100 kW for 8 hours.

$$q_{oven} = P_1 t_1 + P_2 t_2 \qquad [8]$$

where:

q_{oven} is the energy required to heat the oven;
P_1 is the electricity consumed during precalcination [12 kW];
t_1 is the duration of the precalcination step [12 hours];
P_2 is the electricity consumed during the heating step [100 kW]; and
t_2 is the duration of the heating step [8 hours].

Note that it is unlikely that power would need to be supplied at the same levels over the entire 8-hour reaction once the reactor was at temperature. This estimate therefore serves as an upper bound for energy consumption. Material consumption for this reaction is based on stoichiometry.

2.1.4   Oxygen and Lithium Hydroxide

Electricity consumption in the separation of air to produce oxygen was determined from the National Energy Technology Laboratory (NETL) (2007) to be 1.1 mmBtu/ton O_2. This value is very close to that reported by Franklin Associates (2011), 1.3 mmBtu/ton O_2.

In a previous report (Dunn et al. 2014), we describe the co-production of lithium carbonate (Li_2CO_3) and lithium hydroxide (LiOH) at a facility in Nevada. Table 2 and Table 3 detail the energy consumption and emissions generated in this process, which are allocated between the co-products on a mass basis.

Table 2   Purchased Energy Consumption during LiOH and Li$_2$CO$_3$ Production in Nevada[a]

Equipment	Energy Consumption (mmBtu/ton LiOH)	Fuel
Two boilers	32	Residual oil
Dryer	1.9	Propane
Pumps	2.0	Off-road diesel
Mobile equipment	3.3	Off-road diesel
Total	39	

[a]   Sources: Garrett (2004); NCNR (2010).

Table 3   Emissions from LiOH and Li$_2$CO$_3$ Production in Nevada

Pollutant	Emissions (g/ton LiOH)
Material Handling: PM$_{10}$[a]	844
Combustion: [b] PM$_{10}$[c]	126
SO$_2$	0.76
NO$_x$	115
CO	19
VOC	2.4

[a]   Emissions from material handling operations including pond liming, soda ash conveying, lithium carbonate lime system, transfer conveyer, warehouse bin, milled Li$_2$CO$_3$ air classifier system, Li$_2$CO$_3$ handling, lime handling, and LiOH packaging.

[b]   Combustion in the propane-fired rotary dryer. Other fossil fuel combustion emissions are calculated in GREET from the fuel throughput.

[c]   PM = particulate matter; SO$_2$ = sulfur dioxide; NO$_x$ = nitrogen oxide; CO = carbon monoxide; and VOC = volatile organic compound.

2.2 Preparation of LiFePO$_4$ and Production of Its Precursors

For the production of LFP, we compared two alternative preparation techniques: hydrothermal and solid state. Although the solid-state technique occurs at a higher temperature, the hydrothermal technique requires the heating of water in addition to the reactants. The following sections describe these two pathways, as well as material and energy flows for LFP precursors.

2.2.1 Hydrothermal Synthesis of LiFePO₄

Figure 3 depicts the full pathway for the hydrothermal preparation of LFP. Material and energy flows for LiOH (Section 2.1.4) and phosphoric acid (Johnson et al. 2013) are provided elsewhere. The steel industry produces iron sulfate ($FeSO_4$) as a waste product (Stolzenberg 2004). We therefore did not assign energy or environmental burdens to its production.

The following subsections provide material and energy flows for each of these steps.
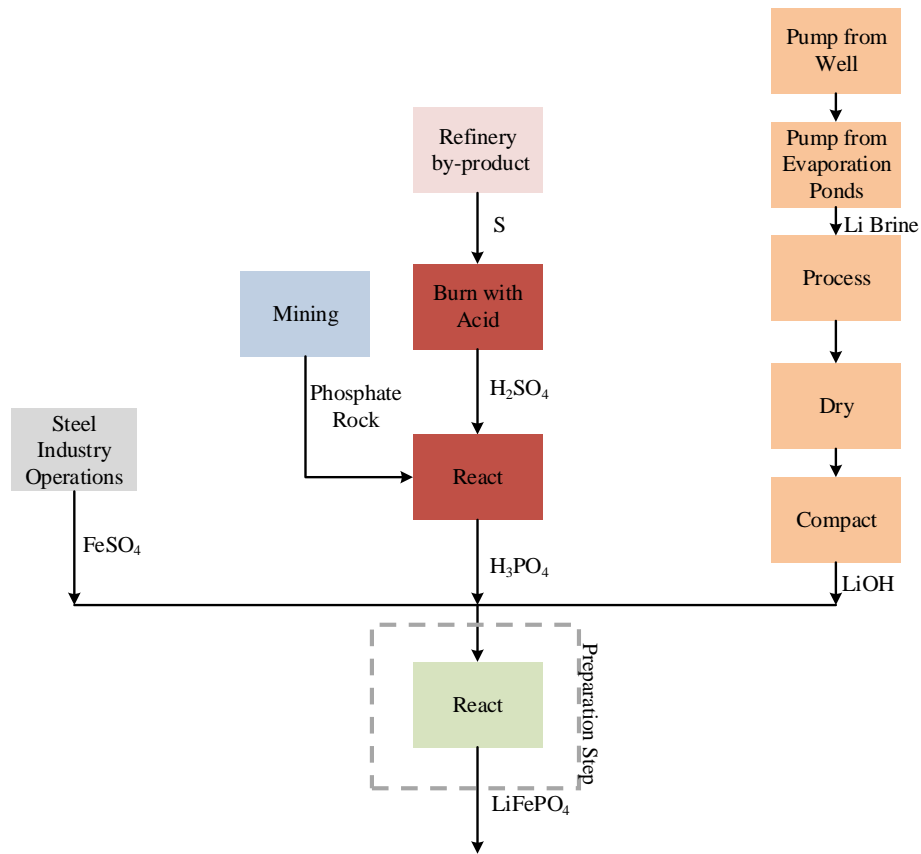
Figure 3 Cradle-to-Gate Preparation of LFP with a Hydrothermal Preparation Step

We again based our calculation of energy consumed in the preparation step itself on the approach of Majeau-Bettez et al. (2011) following Equations 3–5. To calculate q_{CSTR}, we used the parameters in Table 4. Majeau-Bettez et al. (2011) used data from Chen and Whittingham (2006) to develop the parameters in their analysis. These researchers used an autoclave reactor that was not stirred. Therefore, we do not include q_{stir} in our estimation of the energy consumed during hydrothermal preparation of LFP.

Table 4 Parameters for Equations 3–5 for the Hydrothermal Preparation of LFP (Source: Majeau-Bettez et al. 2011)

Parameter	Value
x	0.1 m
A	25 m^2
λ	0.04 W/(m K)
T_0	50°C
T_r	200°C
t	5 hours

Equation 5 was used to calculate the energy required to heat the reactants from 25°C to 200°C. We assumed that the reactant mixture is mostly water and used the average heat capacity of water at the temperature endpoints. As with the hydrothermal preparation of NMC, we estimated that half of the energy used to heat the solution was recovered. The total required energy per ton of LiFePO$_4$ was calculated by assuming an initial concentration of FeSO$_4$ of 22 g/L, that 1 mole of FeSO$_4$ was required to produce 1 mole of LiFePO$_4$, and that the reaction proceeds to completion (Majeau-Bettez et al. 2011; Chen and Whittingham 2006). A co-product forms in this reaction (see Equation 9). For every mole of LFP formed, 1 mole of Li$_2$SO$_4$ forms. Raw material and energy consumption were allocated between these two products on a mass basis. The resulting energy consumption for the preparation step is 31 mmBtu/ton LFP.

$$3LiOH_{(aq)} + H_3PO_{4\,(aq)} + FeSO_{4\,(aq)} \rightarrow LiFePO_{4\,(S)} + Li_2SO_{4\,(aq)} + 3H_2O \qquad [9]$$
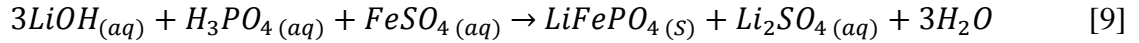
2.2.2 Solid-State Synthesis of LiFePO$_4$

Alternatively, LFP can be produced by a solid-state reaction (Equation 10). The cradle-to-gate pathway for this approach is shown in Figure 4. We selected a solid-state preparation method patented by Dai et al. (2012). Their method combines a lithium compound, an iron compound, and a phosphorous compound. We selected Li$_2$CO$_3$ as the lithium compound. Material and energy flow for this compound are in Dunn et al. (2014). We chose diammonium phosphate (DAP) as the phosphorous compound; GREET data for this compound are documented in Johnson et al. (2013).

$$3Li_2CO_3 + 2Fe_3O_4 + 6(NH_4)_2HPO_4 \rightarrow 6LiFePO_4 \qquad [10]$$
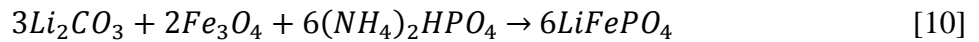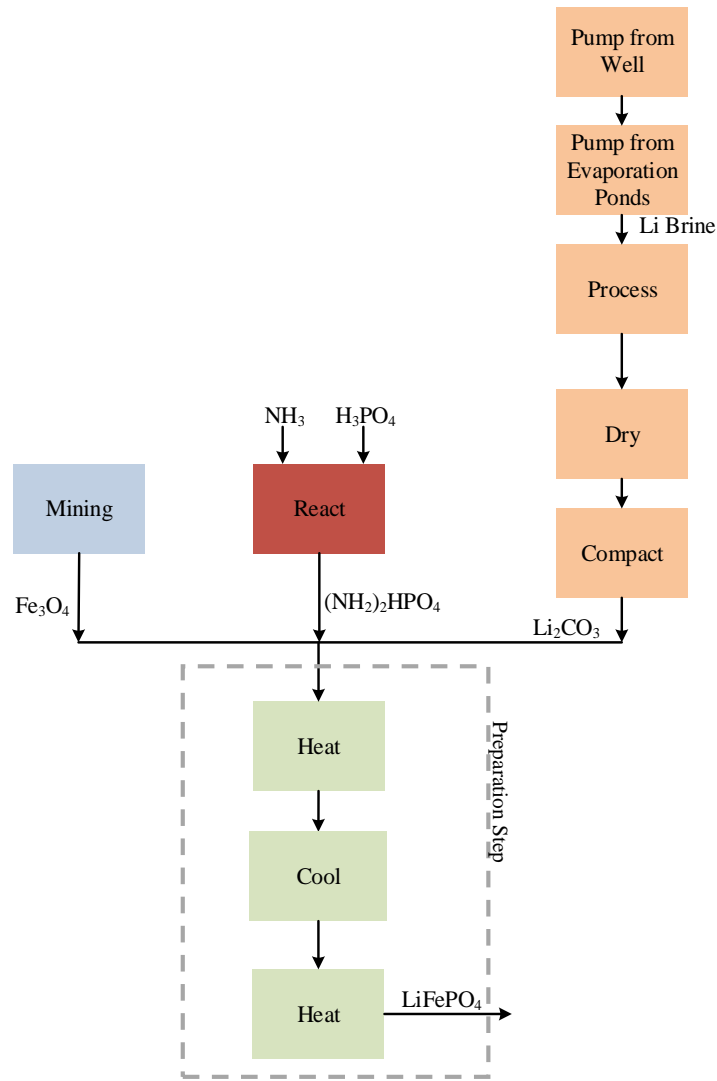
Figure 4   Cradle-to-Gate Preparation of LFP with a Solid-State Preparation Step

The iron compound we selected, Fe_3O_4, or magnetite, is mined. Luossavaara-Kiirunavaara Aktiebolag (LKAB) in Sweden is one company that mines this compound. In 2011, LKAB produced approximately 25 million tons of magnetite pellets (LKAB 2011). Table 5 contains the energy consumed during these operations. The resulting total energy consumed (0.69 mmBtu/ton) is lower than the 2.0 mmBtu/ton processed and pelletized iron ore reported in Keoleian et al. (2012) but higher than the 0.054 mmBtu/ton taconite mined reported in Burnham et al. (2006). Given regional variations including ore grade and changes in technology with time, however, these values are in reasonable agreement.

**Table 5   Energy Consumed in the Mining of Magnetite Pellets
(Source: LKAB 2011)**

Energy Type	Amount Consumed (mmBtu/ton)
Diesel	0.11
Residual oil	0.16
Electricity	0.41
Total	0.68

The solid state LFP synthesis process itself comprises three steps. First, the mixture is heated to between 500°C and 700°C. Then, it is cooled to room temperature. Finally, it is reheated to between 700°C and 900°C to produce the final product. We approached energy consumption calculations for this process as we did those for the solid-state preparation of NMC and used Equations 6–8. We assumed that the first and second heating stages occur at 600°C and 800°C, respectively. We used a heat capacity for the solid mixture of 1.05 $\frac{J}{g \cdot °C}$ for each phase of heating for Equation 7. To calculate q_{oven}, we used the parameters in Table 6 in Equation 8.

**Table 6   Parameters for Equation 8 for the
Solid-State Preparation of LFP
(Source: Dai et al. 2012)**

Parameter	Value
P_1	50 kW
t_1	13
P_2	100 kW
t_2	13

As with the solid-state preparation of NMC, we assumed that an 8,300-L chamber furnace with 33% efficiency was used. To calculate the amount of energy required per kg of LiFePO$_4$ produced, we next assumed that the volume of the mixture did not change and that the reaction proceeded to completion. The density of LiFePO$_4$ was assumed to be 3.6 g/mL (Wilcox et al. 2007). This reaction was assumed to proceed to completion, and the consumption of the reactants was assumed to be stoichiometric. In total, the purchased energy, all electricity, consumed in the preparation step was 2.53 mmBtu/ton.

2.3   Preparation of LiCoO$_2$ and Production of Its Precursors

As with our examination of LFP, we considered both hydrothermal and solid state preparation techniques for the production of LCO. We describe each of these routes in the following subsections.

2.3.1   Solid State Production of LiCoO₂

Figure 5 diagrams the solid-state technique modeled for producing LCO, which entails calcining a compressed mixture of Co_3O_4, a lithium compound (Li_2CO_3), and water (Nakamura et al. 2000) at 725°C. Li_2CO_3 material and energy flow data are detailed in Dunn et al. (2014).

Cobalt oxide (Co_3O_4) was assumed to be produced from heating a stoichiometric amount of CoO from room temperature (25°C) to 900°C (Richardson 2003). GREET already contains energy consumption and emissions associated with CoO mining. The heat capacity of CoO was necessary to use Equation 7 and calculate the heat consumed in producing Co_3O_4. The average heat capacity at the final and initial temperatures in the CoO heating process was used (NIST). We assumed that the heating energy would be provided by a natural gas-fired, 80% efficient furnace. The resulting energy consumed to produce Co_3O_4 is 0.67 mmBtu/ton.
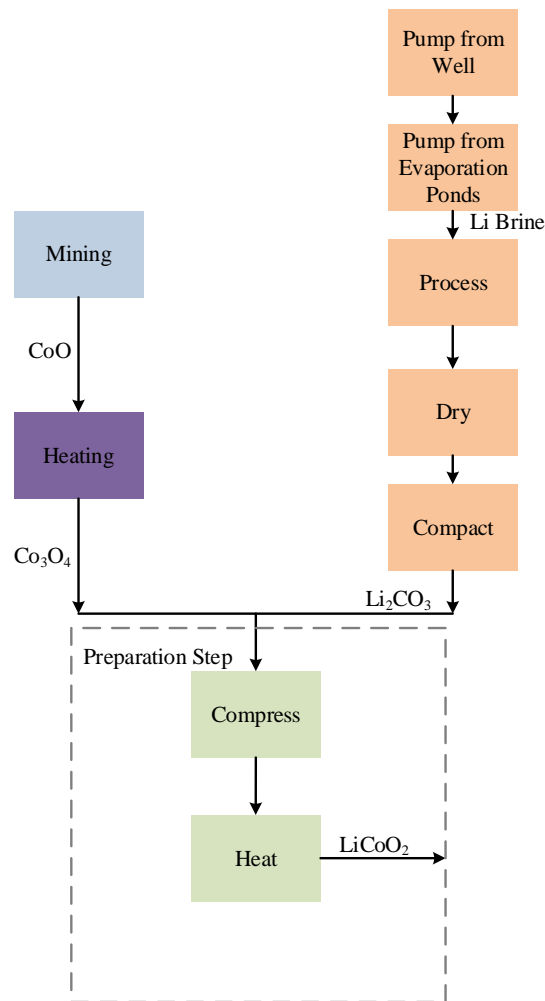
Figure 5   Cradle-to-Gate Preparation of LCO with a Solid-State Synthesis Step

For the preparation step itself, we followed the same approach as we have used for the solid state preparation of NMC and LFP (see Equations 6–8). The furnace volume was set at 8,300 L, its efficiency at 33%. The calcining step was assumed to take place at 725°C for 6 hours, drawing 81 kW. It was necessary to determine the amount of product mass generated within the 8,300-L reactor. In this calculation, we assumed that 1% of the total mass of the input to the calciner was water and that the density of the molded mixture was 1.5 g/mL (Nakamura et al. 2000). (These assumptions, based on the patent, allowed for calculation of the reactants and therefore the products.) We also assumed that the Co_3O_4 and Li_2CO_3 were reacted at molar ratio and the reaction proceeded to completion.

The calcination step for energy consumption was calculated with Equation 7 using a C_p of 1.05 $\frac{J}{g \cdot °C}$ and a change in temperature of 700°C. In summary, the total amount of purchased energy (electricity) consumed in the production of $LiCoO_2$ in the solid-state synthesis step is 1.20 mmBtu/ton. During the calcination step, 204,145 g CO_2/ton are emitted from burning off of the carbonate group in Li_2CO_3.

2.3.2 Hydrothermal Synthesis of LCO

The hydrothermal route to LCO has several precursors that have been discussed in this document or other cited references (e.g., HCl, LiOH, NaOH) and several unique precursors for which we develop material and energy flow data in the following subsections. Figure 6 sketches out the cradle-to-gate pathway for this cathode material prepared hydrothermally (Ado et al. 2002).
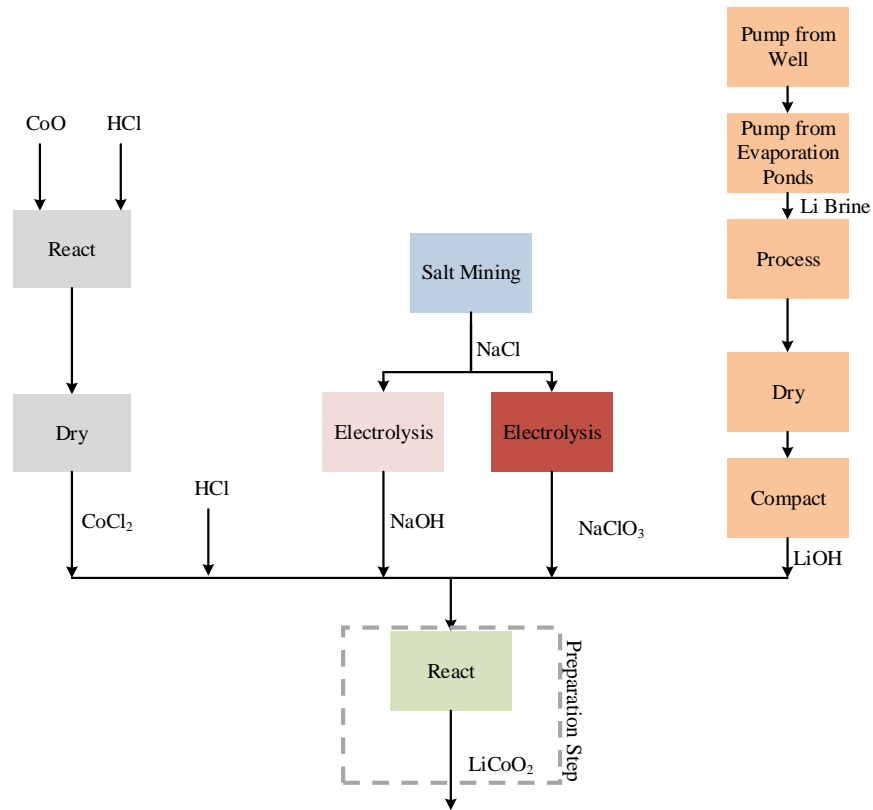
Figure 6   Cradle-to-Gate Preparation of LCO with a Hydrothermal Synthesis Step

2.3.2.1   *Production of CoCl₂*

Richardson (2003) describes a process, outlined in Figure 7, which produces $CoCl_2$ from a reaction between HCl and CoO. A drying step is needed to remove the co-produced water. To calculate the energy consumed in this process, we calculated the energy demand for each of the three heating steps with Equation 7. Although heat capacity data for aqueous solutions of $CoCl_2$ exist, these data are for significantly more dilute solutions (Spitzer et al. 1978). We therefore used a weighted average heat capacity for $CoCl_2$ and H_2O for each step. The process has a low energy intensity of 0.4 mmBtu/ton $CoCl_2$.
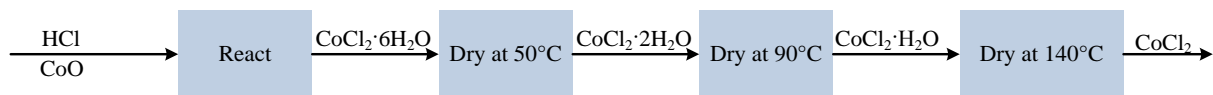
Figure 7 Cradle-to-Gate Production of CoCl₂

2.3.2.2 Production of Sodium Chlorate

Sodium chlorate ($NaClO_3$) is produced from sodium hydroxide (Schlag 2012). Hydrogen is a co-product. The total energy consumed in the process was allocated between hydrogen and sodium chlorate on an economic basis as shown in Equation 10.

$$E_{NaClO_3} = \frac{E_{Total}}{M_{Total}} \times \frac{c_{NaClO_3} m_{NaClO_3}}{c_{NaClO_3} m_{NaClO_3} + c_{H_2} m_{H_2}}$$ [10]

where:

E_{NaClO_3} is the energy intensity of sodium chlorate production;
E_{Total} is the total process energy consumed (17 mmBtu/ton product);
M_{Total} is the total mass of products (H_2 and $NaClO_3$) (1.1 ton);
c_{NaClO_3} = the cost per ton of $NaClO_3$ ($645/ton);
m_{NaClO_3} is the mass of $NaClO_3$ produced (1 ton);
c_{H_2} is the cost of H_2 ($1,580/ton) (DOE 2012); and
m_{H_2} is the mass of H_2 produced (0.06 ton).

Economic allocation provided more reasonable results than the displacement co-product handling technique in which the sodium chlorate receives credit for displacing hydrogen production from natural gas. This latter technique produced distorted results given that hydrogen production is energy intensive. Mass allocation was similarly unsuitable because of the low mass of hydrogen, which belies its economic importance. Energy allocation was not possible because sodium chlorate is not an energy product. With economic allocation of burdens among co-products, we calculated that production of one ton of $NaClO_3$ consumes 14 mmBtu/ton.

Consumption of the raw material, NaCl (Schlag et al. 2008), was also allocated between $NaClO_3$ and the hydrogen by-product by economic allocation. The resulting value is 0.49 ton NaCl/ton $NaClO_3$. GREET values for NaCl production derive from Franklin Associates (2011).

2.3.2.3 Hydrothermal LCO Preparation

The calculations to estimate the energy intensity of hydrothermal LCO preparation follow those of the hydrothermal preparation of LFP and NMC. Table 7 lists the parameters used in Equations 3–5 in the case of LCO. To calculate the energy consumed in heating the water for the reaction, we used the reactor loading rates of water and $CoCl_2 \cdot 6H_2O$ provided in Ado et al. (2002) and assumed the ratio of $CoCl_2$:$LiCoO_2$ would be 1:1. Material demand for LiOH was also based on stoichiometry. Amounts of $NaClO_3$ (the oxidizing agent) and NaOH (which helps the oxidizing agent dissolve) were based on Ado et al. (2002). We assumed that in a full-scale process, the reaction medium would be recycled after precipitation of LCO such that 90% of NaOH would be recycled. The corresponding energy intensity of hydrothermal preparation of LCO was 29 mmBtu/ton. In addition, 99.7% of the purchased energy is natural gas.

Table 7   Parameters for Equations 3–5 for the Hydrothermal Preparation of LCO in a 10,000-L Reactor

Parameter	Value
X	0.1 m
λ	0.04 W/(m K)
T_0	50°C
T_r	225°C
T	2 hours

2.4   Preparation of LMR-NMC and Production of Its Precursors

This cathode material is relatively new and is not in high-volume production (Thackery et al. 2007). Many different preparation methods are reported in the literature (e.g., Wang et al. 2009, Kang et al. 2006). Figure 8 shows the pathway from raw material to final product for LMR-NMC that has been adopted in this analysis. Variations of this process include production by co-precipitation (Gallagher et al. 2011) using different metal oxide precursors (Kang et al. 2006) and pelletizing intermediates, among others. To reiterate, the energy consumption estimates developed in this report are to serve as first estimates of the impacts of producing these cathode materials for batteries and are subject to considerable uncertainty.
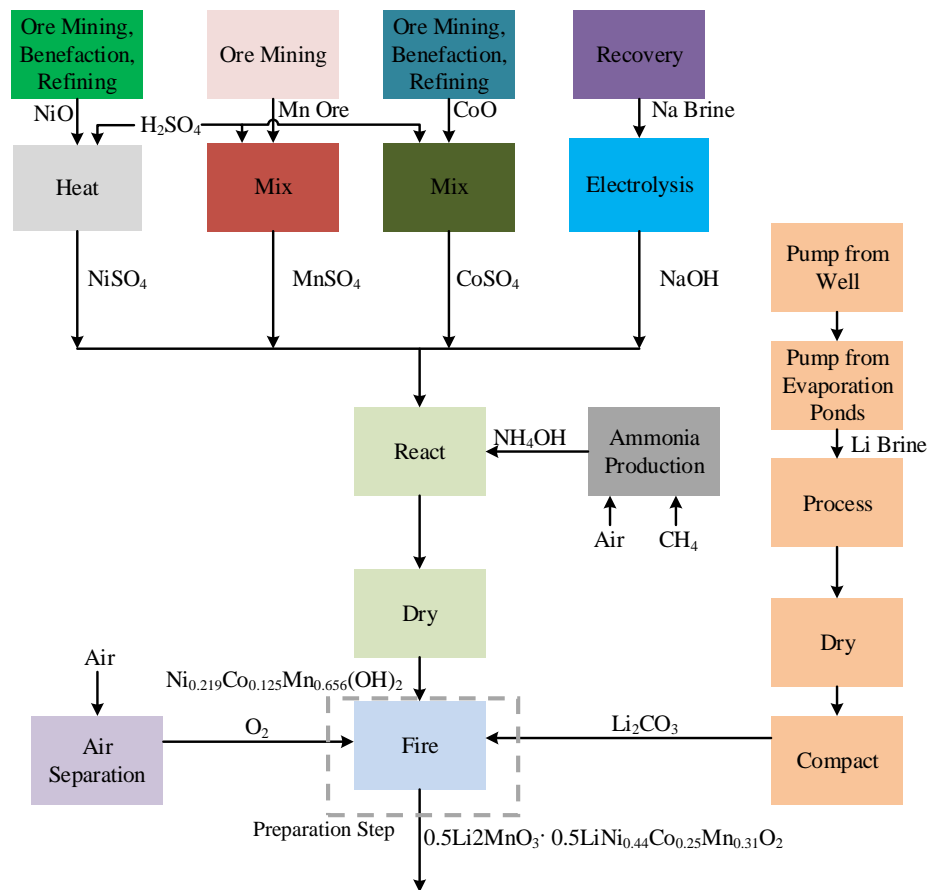
Figure 8 Firing Process for Producing $0.5Li_2MnO_3 \cdot 0.5LiNi_{0.44}Co_{0.25}Mn_{0.31}O_2$

We estimated that the preparation of the metal hydroxide precursor to LMR-NMC has the same energy intensity as that of preparing $Ni_{0.4}Co_{0.2}Mn_{0.4}(OH)_2$ (Section 2.1.2). The resulting energy consumption (1.4 mmBtu/ton, 90% natural gas) was slightly different than that reported in Section 2.1.2 because of the slightly different amounts of metals between the two compounds.

The preparation of the cathode material was assumed to occur through firing at 900°C of the metal hydroxide precursor and lithium carbonate in an oxygen-rich environment (Wang et al. 2009). On the basis of an estimate of the energy intensity of calcining (Dunn et al. 2014), we estimate the energy intensity of this process to be 3.0 mmBtu/ton LMR-NMC.

2.5 Preparation of Graphite

In 2012, the U.S. produced 141,000 t of synthetic graphite, and imported 122,000 t of synthetic graphite, mostly in the form of graphite electrodes, from Japan (25%), China (18%), Canada (14%), India (13%), Russia (11%), Mexico (10%) and other countries. In contrast,

domestic production of natural graphite is nonexistent, while U.S. imported a total of 56,700 t of natural graphite in 2012, 35% from Mexico, 33% from China, 21% from Canada, and the rest from other countries (USGS 2012).

The consumption of natural graphite was for refractories, foundries, and crucibles (39%); metallurgical uses (28%); parts and components (10%); lubricants (9%); batteries (9%) and other uses (5%), whereas high-purity synthetic graphite is mainly used as a carbon raiser additive in iron and steel (USGS 2012).

As of 2010, natural graphite is the preferred anode material for LIBs due to its significantly lower cost compared with synthetic graphite, and represents over half of the LIB anode market (Yoshino 2014). The large battery plant Tesla proposed to build is going to use natural graphite primarily as the anode material (The Gold Report 2014). However, considerable amount of synthetic graphite is also used in LIBs, and its market share is expected to grow (Shaw 2013), because of its better electrochemical performance, and resource security concerns (USGS 2012).

2.5.1 Synthetic Graphite Manufacturing

Synthetic graphite is generally made from pet coke and coal tar pitch (Jäger et al. 2010). Pet coke is typically produced from delayed coking of residues from the thermal processing of crude oil (Predel 2014), while coal tar pitch, derived from coal, is often a byproduct from the coke oven for steel production (Blümer et al. 2011). Coal tar pitch Pet coke is the main raw material, and coal tar pitch serves as the binder, with an average content of 15-30% (Jäger et al. 2010).

Coke produced from coal out of a coke oven can also be used as the primary raw material. However, it would lead to nitrogen puffing problems (irreversible expansion due to release of nitrogen) during the graphitization process, and therefore is not considered in this analysis (Jäger et al. 2010).

The industrial production process for synthetic graphite is depicted in Figure 1. The process starts with grinding and sizing the petroleum coke. Once the milled product meets the grain size requirement, which varies depending on the final application of the synthesized graphite, the ground coke is sent to the mixer to be blended with the coal tar pitch in the desired proportions. The mixers are heated to keep the coal tar pitch in liquid state, allowing the pitch to partially penetrate the pores of the coke during mixing. The mixture coming out of the mixer is cooled from 160-170 °C to around 100°C, and then fed into an extruder or a press for subsequent forming. The purpose of forming is to maximize the density of the mixture and shape the mixture into the form and size of the final product as close as possible. The formed product is subsequently heated to 800-1000 °C in a natural gas-fired furnace. During this baking (sometimes also referred to as carbonization) process, which usually lasts 18-24 h, the coal tar pitch is converted into coke, accompanied by a 30-40% weight loss. To improve the properties of the final graphite, often the baked mixture is impregnated with pitch and rebaked before it is sent to the graphitization furnace. In the graphitization furnace, which is exclusively powered by electricity, the mixture is slowly fired to around 3000 °C for the formation of graphite crystals.

This process typically takes 3-5 days in Acheson furnaces. Adding cooling time, the whole cycle can take up to 3 weeks. Depending on final application, the manufactured graphite may undergo subsequent refining, machining, coating and other processes before distribution.
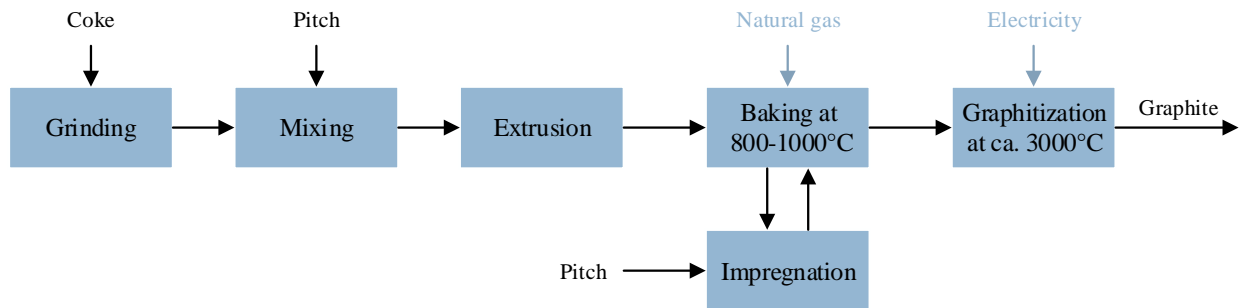
Figure 9. Process Flow Chart for Synthetic Graphite Production

2.5.2 Material and Energy Inputs to Synthetic Graphite Production

The starting materials are assumed to be 80% petroleum coke and 20% coal tar pitch, as reported by a synthetic graphite manufacturer (Tamashausky 2006). Assuming a 90% carbon content for coke (Jäger et al. 2010), a 40% weight loss for the coal tar pitch during baking (Hupp et al. 2003), and not considering other losses, the material inputs for 1 kg synthetic graphite are calculated to be 0.95 kg coke and 0.24 kg pitch. This translates into an overall conversion rate of ~83%, and is in agreement with Notter et al., who reported a material input of 1.2 kg coke per kg graphite, citing personal communication with a major synthetic graphite manufacturer in Europe (Notter et al. 2010).

Energy consumption for synthetic graphite production has been reported in a few LCA studies. Notter et al. added 1.2 kg coal and 1 kWh electricity to the LCI of natural graphite production to represent the production of 1 kg of synthetic graphite (Notter et al. 2010). The energy input of 1 kWh/kg (3.10 MMBtu/ton) was derived from thermodynamic calculation, assuming an initial temperature of 20°C, a final temperature of 2800°C, a constant specific heat of 1.15 kJ/(kg.K), and an additional 10% heat to hold the temperature in the furnace (Hischier et al. 2009). Based on the polynomial describing specific heat as a function of temperature (Butland and Maddison 1973), the specific heat of graphite is 0.69 kJ/(kg.K) at 20°C , and 2.23 kJ/(kg.K) at 2800 °C. The assumed constant specific heat of 1.15 kJ/(kg.K) by Notter *et al* was not a good approximation, and the rationale behind this assumption was not clear. In addition, their calculation did not take into account the efficiency of the furnace. Therefore, their estimate of energy consumption is not considered in this analysis. In another study, Majeau-Bettez *et al* approximated the production of synthetic graphite by carbon anode baking of the aluminum industry, and estimated the energy requirement to be 4.8-5.2 MJ/kg (4.13-4.47 MMBtu/ton) (Majeau-Bettez *et al* 2011). However, carbon anodes for aluminum smelters are typically produced from coal pitch and pet coke by heating the mixture at 1000-1200°C (Frank et al. 2012). Therefore, carbon anode baking is fairly representative of the baking stage for synthetic graphite production, but does not account for the energy requirement of the graphitization

process. For this reason, the energy consumption estimate by Majeau-Bettez et al. is not used in this analysis either.

Baking and graphitization are the two most energy-intensive processes in graphite synthesis. The baking furnace is fueled by natural gas, whereas the graphitization furnace is electric (Jäger et al. 2010). Assuming variable specific heat for graphite (Butland and Maddison 1973), thermodynamic calculations return a theoretical heat demand of 1.50 MJ/kg (1.29 MMBtu/ton) and 4.25 MJ/kg (3.66 MMBtu/ton), for baking and graphitization processes respectively.

The average electricity consumption of an Acheson furnace, which is the mainstream graphitization furnace, is estimated to be 4.5 kWh/kg, or 16.2 MJ/kg (13.93 MMBtu/ton) of graphite (Hupp et al. 2003). Dividing the theoretical energy requirement of 4.25 MJ/kg (3.66 MMBtu/ton) by the industry average of 16.2 MJ/kg (13.93 MMBtu/ton) electricity input, the net efficiency for the graphitization process is estimated to be around 26%. This is consistent with the case of silicon carbide production, which is another industrial process utilizing the Acheson furnace (Guichelaar 1997). The Acheson process to produce silicon carbide involves heating silicon sand and ground coke at 2200-2700 °C for a prolonged period. The theoretical specific energy requirement for this process is estimated to be 2.2 kWh/kg (6.81 MMBtu/ton), while the actual electricity consumption ranges from 6 kWh/kg to 12 kWh/kg (Gupta et al. 2001), which corresponds to a net efficiency of 36.6% and 18.3%, respectively. Although the 26% efficiency is lower than the thermal efficiency of non-regenerative electrical furnaces, which typically ranges from 35% to 50% (Dryden 1982), it seems reasonable, as the energy needed to maintain the temperature after the initial heating is not accounted for in the thermodynamic calculation.

The amount of energy consumed by the baking furnace and the furnace efficiency is not reported in literature. Considering the lower temperature and the shorter cycle time for the baking process, although additional heat is also needed to maintain the baking temperature after the initial heating, this additional heat requirement and the heat loss may be moderate compared with that of graphitization. The efficiency for the baking furnace is therefore assumed to be 25%, which is typical of natural gas furnaces used in the metal and glass industries (Dryden 1982, DOE 1999).Since baking is where the weight loss predominantly happens, factoring in the 83% conversion rate, and the 25% efficiency of the furnace, the natural gas intensity of the baking process is approximately 6.0 MJ/kg (5.15 MMBtu/ton) of produced graphite.

It should be noted that, the energy consumption estimated for the baking process could be on the higher end, due to the use of the specific heat of graphite as a substitute for that of coke and pitch, which is reportedly lower (Long et al. 2015). The reason for the substitution is that no reliable variable specific heat data was available for coke and pitch.

Both coal tar pitch and pet coke contain impurities such as sulfur, nitrogen and ash. When calcined, these impurities would burn off and result in emissions of criteria pollutants. These emissions are mostly from the baking stage, and can be estimated from stoichiometric calculation based on the impurity contents for coal tar pitch and pet coke. In this analysis, it is assumed that coal tar pitch has a hydrogen content of 5%, an oxygen content of 2%, a nitrogen content of 1.3%, a sulfur content of 0.8%, and an ash content of 0.3% (Blümer et al. 2011) , whereas pet

coke has a sulfur content of 3.5% and an ash content of 0.4% (Predel 2014). It is also assumed that all nitrogen will be converted into NO_2, sulfur into SO_2, and ash into PM. As aforementioned, 10% and 40% of weight loss is expected during baking for pet coke and coal tar pitch respectively. Subtracting the contents of known impurities, the remaining weight loss of 6.1% for pet coke, and 30.6% for coal tar pitch is attributed to the volatilization of volatile combustible matter, which is assumed to be carbon and is released as CO_2 during baking.

2.5.3 Summary of Material and Energy Flow for Synthetic Graphite Production

The estimated material input, energy input and emissions for synthetic graphite production is summarized in Table 8. The production is assumed to be based in China, so Chinese national grid mix is used for the electricity consumption. As mentioned earlier, carbon anode baking can serve as a good surrogate for the baking stage. For comparison purpose, the energy consumption and process emissions for carbon anode production as reported by the Aluminum Association (The Aluminum Association 2013) are listed alongside our own estimates for graphite baking. It should be noted that our estimates of process emissions do not account for emission control technologies, whereas the Aluminum Association reported controlled emissions.

Table 8   Material and Energy Inputs for the Production of 1 ton of Synthetic Graphite

	Carbonization	Carbon anode baking (The Aluminum Association 2013)	Graphitization
Material inputs (ton/ton)			
Pet coke	0.95	0.99	---
Coal tar pitch	0.24	0.22	---
Purchased energy inputs (MMBtu/ton)			
Residual oil	---	1.8	---
Diesel	---	0.33	---
Natural gas	5.1	2.4	---
Electricity	---	0.57	14
Total	5.1	5.2	14
Non-combustion Emissions (g/ton)			
NO_x	9,300	760	---
PM	4,100	320	---
SO_x	64,000	4,100	---
CO_2	440,000	150,000	---

It is worth mentioning that currently, synthetic graphite is predominantly (>85%) consumed as electrodes in electric arc furnaces for steel production (Jäger *et al* 2010 and Hupp *et al* 2003). Graphite electrodes are primarily produced from needle coke, as opposed to the pet coke that we assumed in this analysis (Adams et al. 2007). One manufacturer of synthetic graphite also uses needle coke as the filler material for their high-quality graphite products (Tamashausky 2006). Needle coke is produced by calcining pet coke at ca. 1300°C under

reducing conditions in kilns (Jäger et al. 2010). This pet coke calcination process may entail additional energy consumption. However, it was not clear how the use of needle coke instead of pet coke would affect the graphitization process, especially in terms of energy requirement. In absence of good data, pet coke is assumed as the raw material for synthetic graphite for LIB applications. This assumption should be revisited when data on synthetic graphite production from needle coke becomes available.

At times, graphite may be blended with silicon to form the anode material. GREET contains a battery design that pairs a Gr/Si anode mix with the LMR-NMC cathode. Material and energy flow data used in GREET for silicon production is in Benavides et al. (2015).

2.6 Preparation of Metallic Lithium as an Anode Material

Lithium is primarily produced from continental brines and pegmatites (mainly spodumene), with continental brines as the dominant and most economical lithium source (USGS 2013a). In 2013, the United States produced 870 metric tons of lithium from one brine operation in Nevada, and imported 2,210 metric tons of lithium, among which 50% was from Chile, and 46% was from Argentina. Both Chile and Argentina produce lithium from brines of salars (Wietelmann and Steinbild 2014). Lithium production from spodumene is mostly based in Australia, although China also produces large quantities of lithium from imported mineral concentrates (Kamienski et al. 2004). Global lithium consumption in 2013 was estimated to be 34,200 metric tons. 35% of consumed lithium was used as flux in ceramics and glass production, 31% was for batteries, 8% in lubricating greases, 6% in continuous casting mold flux powders, 5% for air treatment, 5% in polymer production, 1% in primary aluminum production, and the rest for other uses (USGS 2013a). Due to predicted increase in global lithium consumption, deeper penetration of lithium production from spodumene is expected in the future. Economical lithium production from geothermal and oilfield brines are also under investigation (Wietelmann and Steinbild 2014, Stamp et al. 2012).

It should be noted that the majority of lithium consumed in batteries is in the form of lithium compounds as precursors for cathode materials (Goonan 2012). The production of lithium compounds for the cathode of LIBs are described elsewhere (Dunn et al. 2014). In this section, we focus on the production of metallic lithium, which is a promising anode material for LIBs (Brodd 2009), and is the proposed anode material for next-generation batteries, such as lithium-sulfur (Wang et al. 2011), and lithium-air batteries (Girishkumar et al. 2010).

2.6.1 Metallic Lithium Production from Brine

The process of metallic lithium production from brine is shown in Figure 10. Lithium carbonate production from brine needs to be adapted to each salar based on Li concentration, Li/Mg ratio, evaporation rate, etc. In Chile, in the Atacama region, brines are pumped to a series of solar ponds for salts to crystalize successively before the brine reaches the final concentration. At the Silver Peak facility in Nevada, brine is treated with lime to precipitate magnesium before

being pumped to the solar ponds. In the high altitudes at which brine is produced in Argentina, the brine is concentrated through selective adsorption by hydrated alumina-lithium chloride granules before it enters the pond system.
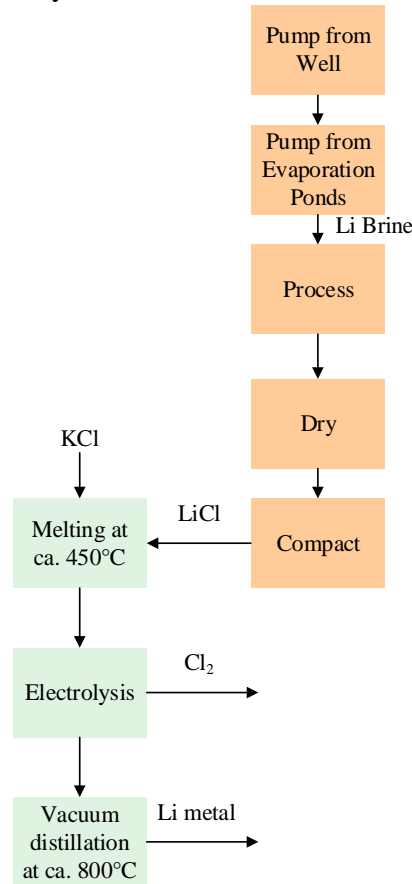
Figure 10 Process Flow Chart for Metallic Lithium Production

The concentrated brine then undergoes additional purification steps to remove impurities of boron, magnesium and calcium. Boron is usually removed by liquid-liquid extraction. The addition of soda ash removes magnesium, and the addition of lime precipitates additional magnesium and sulfate residues. Soda ash is then added to the purified LiCl to form Li_2CO_3. Material and energy flows for Li_2CO_3 in GREET are described in Dunn et al. (Dunn et al. 2014).

The industrial production of metallic lithium is exclusively through electrolysis of molten LiCl. In addition to the cell feed of anhydrous LiCl, KCl is also supplied to the cell as the solvent and supporting electrolyte. The presence of KCl lowers the melting point for the eutectic, so the reaction can occur at ca. 400-460°C. In addition, the decomposition potential of KCl is higher than that of LiCl, which limits the formation of K during the electrolysis process. The theoretical power consumption of the electrolysis process is 14.2 kWh/kg (44.0 MMBtu/ton) lithium, while the actual consumption ranges from 28 to 32 kWh/kg (86.7 to 99.1 MMBtu/ton) lithium (Wietelmann and Steinbild 2014).

Lithium obtained directly from the electrolysis process has a purity of 97-99.5% (Di 2005). Depending on final application of the lithium, further refining may be necessary. Vacuum distillation is one of the common refining technologies for lithium (Yu et al. 2011). The distillation process takes place in an electric chamber at ca. 600-800°C, separating lithium from the impurities through vaporization (Chen et al. 2002).

2.6.2 Calculation of Material and Energy Flows of Metallic Lithium Production

As the production of Li_2CO_3 from lithium brine has been examined in GREET, this analysis only focuses on lithium electrolysis and distillation. LiCl is assumed to be imported from Chile, and the electrolysis and distillation is assumed to be based in the U.S. For the electrolysis process, the eutectic typically contains 35-45 mole percent KCl (Sadoway 1998). However, the consumption of KCl in the electrolysis reaction is not as significant compared with that of LiCl. Material inputs of 6.5 ton LiCl and 1.5 ton KCl are reported in (Di 2005) for the production of 1 ton metallic lithium. For the distillation process, no material input is needed.

In addition to the metallic lithium, the electrolysis process also produces chlorine. To account for this coproduct, mass allocation was applied when compiling material and energy flows pertaining to heating and melting the eutectic, as well as electrolysis, and the amount of chlorine formed per ton of produced lithium was found by stoichiometry. Mass allocation was chosen in this analysis because it is based on physical relationship between the products and is not subject to changes over time. For readers who are interested in exploring economic value-based allocation, the 10-yr average price for chlorine over 2004-2013 is $250/ton (OrbiChem 2013). The price for metallic lithium averaged $71632/ton over 2001-2010 (USGS 2013b).

Electricity consumption for the electrolysis is reported in a few studies (Wietelmann and Steinbild 2014, Di 2005, Sadoway 1998). An electricity input of 32 kWh/kg (99.1 MMBtu/ton) Li (Wietelmann and Steinbild 2014, Di 2005), is assumed in this study, slightly below the 35 kWh/kg (108.3 MMBtu/ton) Li value reported by Sadoway. The energy requirements for heating up the eutectic before the electrolysis and vacuum distillation are estimated by Equation 11.

$$E = (m * C_p * \Delta T + m * L)/\eta \qquad [11]$$

Where:
m represents the mass of lithium;
C_p represents the specific heat of lithium;
ΔT represents the difference between the initial temperature and final temperature of the process;
L represents the latent heat of lithium; and
η represents the efficiency of the furnace used for the process.

The specific heat and the heat of fusion for the LiCl/KCl mixture is obtained from literature (ORNL 1953), the specific heat for liquid lithium is obtained from a NASA report (Davison 1968), and the heat of vaporization for metallic Li is obtained from the Chemistry Webbook database of National Institute of Standards and Technology (NIST). These

thermochemistry data were summarized in Table 9. Assuming an initial temperature of 20°C, a final temperature of 450°C, and a furnace efficiency of 35% (the average efficiency of a natural gas furnace used in the metal casting industry as found on the website of Minnesota Technical Assistance Program by the University of Minnesota), the heat requirement for heating up and melting the eutectic is estimated to be 16.4 MJ/kg (14.1 MMBtu/ton) Li. The furnace is assumed to be fired by natural gas. As the lithium feed to the distillation chamber comes directly from the electrolysis process, an initial temperature of 450°C is assumed for the distillation process. The final temperature is assumed to be 800°C, and 45% (the average efficiency of an electric arc furnace) is used as an approximation for the efficiency of the electric chamber (University of Minnesota 2011). The electricity consumption for the distillation process is then calculated to be 54.3 MJ/kg (40.2 MMBtu/ton) Li.

Table 9 Thermochemistry properties for the eutectic and metallic lithium

	m (kg/kg Li)	T_0 (°C)	T(°C)	$C_{p,1}$(kJ/kg.K)	$C_{p,2}$(kJ/kg.K)	L (kJ/kg)
Heating eutectic	8	20	450	0.964 (up to 351°C)	1.341(T>351°C)	268
Distillation	1	450	800	4.169	---	22,954

2.6.3 Summary of Material and Energy Flow for Synthetic Graphite Production

Material and energy flow data adopted for production of metallic lithium in GREET are summarized in Table 10 . It should be noted that there is substantial uncertainty associated with the energy consumption for the vacuum distillation process. A large consumption of 52 kWh/kg (161.0 MMBtu/ton) Li has been reported (Yu et al. 2011). This value is not used in the analysis because it would not make sense for the refining process to consume more energy than the electrolysis process. Unfortunately, the literature contains very little information about lithium refining and the steps involved in terms of energy consumption. At this point, it is also unclear whether lithium refining is the industry norm, especially for lithium used as anode for LIBs. These data are adopted in GREET to allow users to explore estimates of lithium-containing anodes for lithium ion batteries.

Table 10 Material and Energy Inputs for the Production of 1 ton Metallic Lithium

	Heating and melting the eutectic	Electrolysis	Vacuum Distillation
Material inputs			
LiCl (ton)	6.5	---	---
KCl (ton)	1.5	---	---
Energy inputs			
Natural gas (MMBtu)	14	---	---
Electricity (MMBtu)	---	99	47

3 BATPAC MODELING OF BATTERIES WITH DIFFERENT CATHODE MATERIALS

The amount of cathode material needed in a battery is dependent upon the properties of the cathode material. The BatPaC model takes these properties into account and designs a battery for either an HEV, PHEV, or BEV based on a user-specified cathode material and battery performance parameters that depend on the type of battery being designed (e.g., power or energy). One key purpose of BatPaC is to allow users to change battery chemistries and design requirements to estimate the manufacturing cost of a battery pack in 2020 for either an HEV, PHEV, or BEV. The model represents present-day technology and manufacturing practices, and further assumes it will still be in use in 2020, while it also allows for some efficiency improvements to yield a more energy-dense battery.

BatPaC adopts a prismatic pouch cell structure, as shown in Figure 11. The pouch is made of a trilayer polymer/aluminum material. Aluminum and copper foils serve as the current collectors at the cathode and anode, respectively. The anode is coated on both sides with graphite. The cathode material can be one of five chemistries, as described below. A polymeric binder material holds the active material particles together, and a porous membrane separates the two electrodes. The pores of both this separator and the active materials are filled with an electrolyte, modeled in BatPaC as $LiPF_6$ (lithium hexafluorophosphate) in an organic solvent containing linear and cyclic carbonates. During discharge, the lithium ions move from the anode to the cathode while the electrons travel through the current collectors and the external circuit to perform external work. BatPaC models these cells as being enclosed in a module (Figure 12); there are six modules per battery.
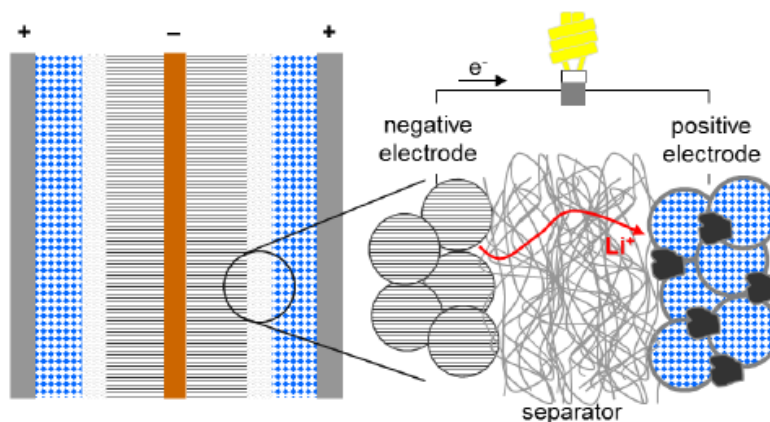
**Figure 11 Cell Chemistry in a Lithium-Ion Battery
(Source: Nelson et al. 2011)**
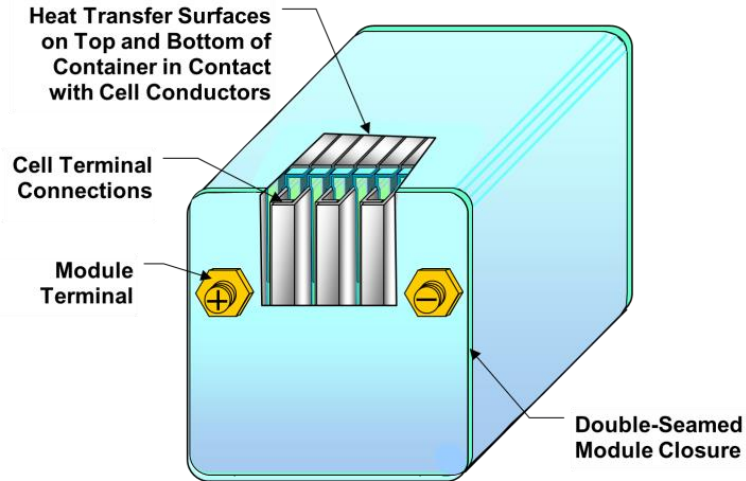
Figure 12 Module Structure (Source: Nelson et al. 2011)

BatPaC users can select from among the following five battery chemistries:
1. Lithium nickel cobalt aluminum oxide with a graphite electrode (NCA-G)
2. Lithium nickel manganese cobalt oxide with a graphite electrode (NMC-G)
3. Lithium iron phosphate with a graphite electrode (LFP-G)
4. Lithium manganese spinel with a titanium dioxide electrode (LMO-LTO)
5. Lithium manganese oxide spinel with a graphite electrode (LMO-G)

For this report, we used BatPaC to calculate the compositions for NMC-G, LFP-G, and LMO-G. In addition, lithium cobalt oxide with a graphite anode and LMR-NMC with a graphite/silicon anode were added to BatPaC and examined. The batteries were model with the parameters summarized in Tables 11-13, developed on the basis of data from Argonne's Autonomie model (Argonne 2011) for mid-sized vehicles in 2015. For PHEV batteries, we ran BatPaC using two different power requirements, 60 kW and 149 kW, in order to model both split and series PHEV batteries. In addition, the numbers of cells in each battery were varied in order to achieve a reasonable voltage based on vehicle type. For HEV batteries, we aimed for the voltage to be around 260 V, whereas for PHEV and EV batteries we aimed for a voltage of about 360 V. The resulting compositions from these models can be found in Appendix A.

Table 11 HEV Parameters from BatPaC

	LMO	NMC	LFP
Power (kW)	30	30	30
Energy (kWh)	2	2	2
Energy Requirement (Wh/mile)	220	220	220
Cells in Battery	72	72	76

Table 12 EV Battery Parameters from BatPaC

	LMO	LCO	NMC	LFP	LMR-NMC
Power (kW)	80, 115, 149	80, 115, 149	80, 115, 149	80, 115, 149	80, 115, 149
Energy (kWh)	28	28	28	28	28
Energy Requirement (Wh/mile)	220	220	220	220	220
Cells in Battery	96	96	96	100	100

Table 13 PHEV Battery Parameters from BatPaC

	Series PHEV			Split PHEV		
	LMO	NMC	LFP	LMO	NMC	LFP
Power (kW)	149	149	149	60	60	60
Energy (kWh)	9	9	9	9	9	9
Energy Requirement (Wh/mile)	220	220	220	220	220	220
Cells in Battery	96	96	100	96	96	100

4 CONCLUSIONS AND FUTURE WORK

With the material and energy flow data entered into GREET, we calculated total (full fuel cycle) energy consumption associated with the production of each of the cathode materials.

Table 14 contains these values and documents the major contributor to total energy consumption, as well as the contribution from the preparation step (the step from which the cathode material is prepared from its immediate precursors), either SS or HT. Production of cobalt-containing cathode materials is the most energy intensive. In cathode materials that contain cobalt or nickel, these compounds contribute the most to the total energy consumed in producing that cathode. For cobalt-containing cathodes, the preparation step contributed less than 15% to the total energy consumption. For cathode materials with a lower overall energy intensity, the preparation method could contribute more than half of the total energy consumption. Hydrothermal preparation techniques were estimated to be more energy intensive than solid state techniques because of the energy consumed in heating the solvent. With the preparation step being a relatively minor contributor to the total energy consumed in cathode production, battery recycling could prove a valuable technique to recover constituent cathode material, such as cobalt, at a lower energy intensity than recovering and processing virgin cobalt.

Table 14 Total Energy Consumed in Preparing Cathode Materials

| Cathode | Energy Consumption (mmBtu/ton) | Preparation Step | | Major Contributor to Energy Consumption | Contribution (%) |
		Energy Consumed[b] (mmBtu/ton)	Contribution to Total (%)		
NMC	135	4.5	3	NiO	40
LMR-NMC	100	3.0	3	CoO	30
LCO (SS)	150	2.6	2	CoO	88
LCO (HT)	251	32	13	CoO	53
LFP (HT)	48	35	71	LFP preparation	71
LFP (SS)	39	6	16	Fe_3O_4	40
LMO[a]	26	15	56	LMO preparation	56

[a] Some minor revisions have been made to GREET data for this pathway. Please see Dunn et al. (2014).

[b] Full fuel cycle energy calculated in GREET from purchased energy values reported herein.

Battery composition varies slightly with cathode type because less of the cathode material is needed in batteries with higher-capacity cathode materials. Figure 13 shows that a BEV battery with LMR-NMC has significantly less cathode material than a battery with LMO because the capacity of LMR-NMC is more than double that of LMO. Comparing 149-kW EV batteries as specified in Table 12 with different cathode materials, the battery with the highest-capacity cathode material, LMR-NMC, has the lowest total mass (Figure 14).
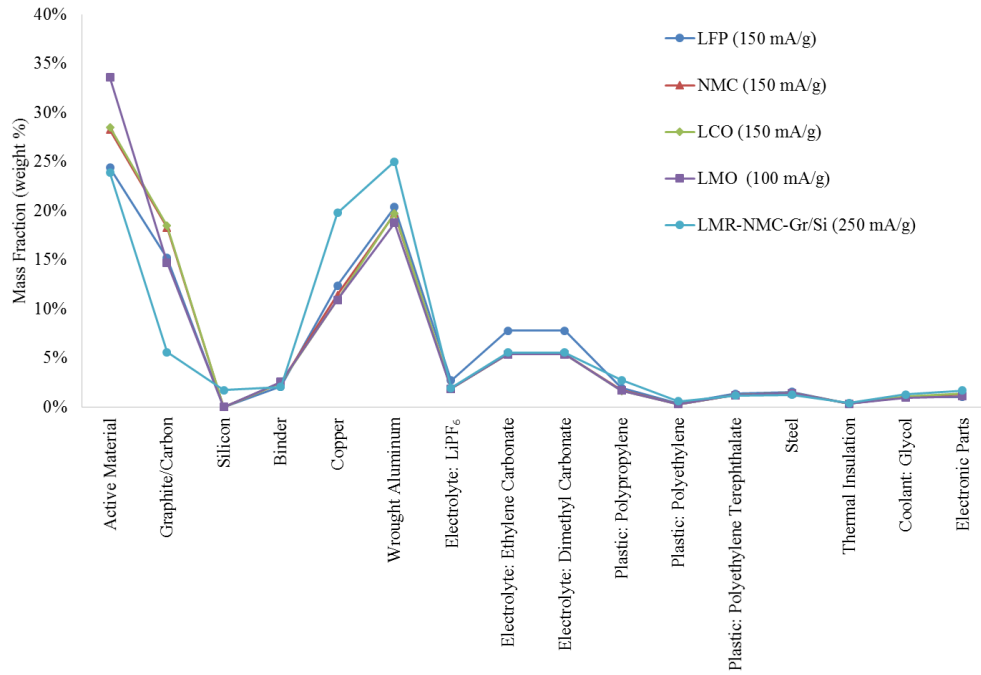
Figure 13   Variation in BEV Battery (149 kW) Composition with Cathode Type
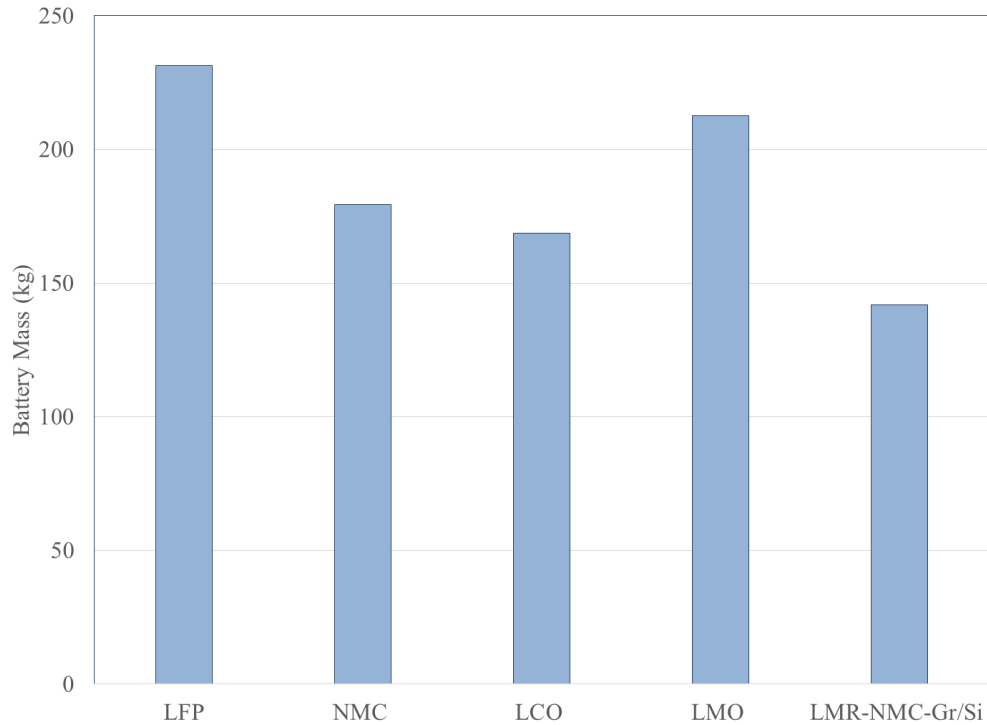
Figure 14   Variation in BEV Battery Mass with Cathode Type

Going forward with this analysis, we will publish a paper with a full analysis of the production of cathodes for lithium-ion batteries and the influence of cathode identity on electric vehicles' life cycle energy consumption and emissions. The paper will also consider the potential of battery recycling to reduce the energy and environmental impacts of cathode and battery production. We will develop more detailed analysis of the production of nickel and cobalt from different types of ores (e.g., sulfide, laterite) by different purification techniques. Further development of lithium ion battery in GREET will focus on other battery components, such as the anode and electrolyte.

5 REFERENCES

Adams, R., Frohs, W., Jäger, H., Roussel, K., 2007. Graphite electrode and needle coke development.
http://acs.omnibooksonline.com/data/papers/2007_D031(K).pdf, accessed July 1, 2015.

Ado, K., M. Tabuchi, H. Kobayashu, and H. Kageyama, 2002, *Process for Producing Layered Rock-Salt Type Lithium Cobalt Oxide by Hydrothermal Oxidation*, United States Patent 6399041, June 4.

Antonsen, D.H., D.T. Meshri, and Updated by Staff, 2005, "Nickel Compounds," *Kirk-Othmer Encyclopedia of Chemical Technology*, Hoboken, New Jersey: Wiley-Interscience.

Argonne (Argonne National Laboratory), 2011, *Autonomie*, [http://www.autonomie.net/.

Benavides, P. T., Dai, Q., Sullivan, J., Kelly, J. C., Dunn, J. B., 2015, "Material and Energy Flows Associated with Select Metals in GREET2: Molybdenum, Platinum, Zinc, Nickel, Silicon,"ANL/ESD-15/11, Argonne National Laboratory, Argonne, Ill.

Blümer, G.-P., Collin, G., Höke, H., 2011. Tar and Pitch, in: Ullmann's Encyclopedia of Industrial Chemistry. Wiley-VCH Verlag GmbH & Co. KGaA.

Burnham, A.B., M. Wang, and Y. Wu, 2006, "Development and Application of GREET 2.7 – The Transportation Vehicle-Cycle Model," ANL/ESD/06-5, Argonne National Laboratory, Argonne, Ill.

Butland, A.T.D., and R.J. Maddison, 1973, "The specific heat of graphite: An evaluation of measurements". *Journal of Nuclear Materials* 49: 45–56.

Brodd, R.J., 2009, "Synopsis of the Lithium-Ion Battery Markets," in *Lithium-ion Batteries, Science and* Technologies, M. Yoshio, R. J. Brodd, A. Kozawa (eds.) Springer.

Chen, J., and M.S. Whittingham, 2006, "Hydrothermal Synthesis of Lithium Iron Phosphate," *Electrochem. Commun.* 8: 855–858.

Chen, W.L., L.Y. Chai, X.B. Min, B. Yang, Y.N. Dai, X. Yu, and C.F. Zhang, 2002, "Vacuum distillation refining of crude lithium. II. Kinetics on vacuum distillation of crude lithium", *Transactions of the Nonferrous Metals Society of China*(China), 12(1): 152-155.

Dai, Q., J. Shen, and F. Xiao, 2012, *Lithium Iron Phosphate Cathode Material*, United States Patent 8088035, January 3.

Davison, H.W., 1968, Compilation of thermophysical properties of liquid lithium.
http://ntrs.nasa.gov/archive/nasa/casi.ntrs.nasa.gov/19680018893.pdf, accessed June 24, 2015.

Di, X.L., Q.S. Pang, and Q. Li, 2005, "Comparative Analysis of Productive Technology for Metallic Lithium". *Journal of Salt Lake Research* 13(2): p. 45-52.

DOE (U.S. Department of Energy), 2012, DOE Hydrogen and Fuel Cells Program Record #12024, September 24.

Dryden, I.G.C. (Ed.), 1982. Chapter 8 - Furnaces: principles of design and use, in: The Efficient Use of Energy (Second Edition). Butterworth-Heinemann, pp. 116–165.

Dunn, J.B.; M. Barnes, L. Gaines, J. Sullivan, and M. Wang, 2014, "Material and Energy Flows in the Material Production, Assembly, and End-of-Life Stages of the Automotive Lithium-Ion Battery Life Cycle," ANL/ESD/12-3 Rev, Argonne National Laboratory, Argonne, Ill.

Dunn, J.B., S. Mueller, M. Wang, and J. Han, 2012a, "Energy Consumption and Greenhouse Gas Emissions from Enzyme and Yeast Manufacture for Corn and Cellulosic Ethanol Production," *Biotechnology Letters* 34: 2259–2263.

Dunn, J.B., L. Gaines, J. Sullivan, and M.Q. Wang, 2012b, "The Impact of Recycling on Cradle-to-Gate Energy Consumption and Greenhouse Gas Emissions of Automotive Lithium-Ion Batteries," *Environmental Science and Technology*, 46: 12704–12710.

Ellingsen, L.A., G. Majeau-Bettez, B. Singh, A.K. Srivastava, L.O. Valøen, and A.H. Strømman, 2014, "Life Cycle Assessment of a Lithium-Ion Vehicle Battery Pack," *Journal of Industrial Ecology* 18: 113–124.

Frank, W.B., Haupin, W.E., Vogt, H., Bruno, M., Thonstad, J., Dawless, R.K., Kvande, H., Taiwo, O.A., 2012. Aluminum, in: Ullmann's Encyclopedia of Industrial Chemistry. Wiley-VCH Verlag GmbH & Co. KGaA.

Fergus, J.W., 2010, "Recent Developments in Cathode Materials for Lithium Ion Batteries," *Journal of Power Sources* 195: 939–954.

Franklin Associates, 2011, *Cradle-to-Gate Life Cycle Inventory of Nine Plastic Resins and Four Polyurethane Precursors*, prepared for the Plastics Division of the American Chemistry Council.

Gallagher, K.G., S. H. Kang, S. U. Park, S. Y. Han, 2011, "$xLi_2MnO_3 \cdot (1-x)LiMo_2$ blended with $LiFePO_4$ to achieve high energy density and pulse power capability," *Journal of Power Sources* 196: 9702-9707.

Garrett, D.E., 2004, *Handbook of Lithium and Natural Calcium Chloride their Deposits, Processing, Uses and Properties*, Elsevier Academic Press, Amsterdam; Boston.

Girishkumar, G., McCloskey, B., Luntz, A.C., Swanson, S., Wilcke, W., 2010, "Lithium−Air Battery: Promise and Challenges", *J. Phys. Chem. Lett.* 1: 2193–2203.

Goonan, T.G., 2012, Lithium use in batteries.
http://pubs.usgs.gov/circ/1371/pdf/circ1371_508.pdf, accessed July 7, 2015.

Guichelaar, P.J., 1997. Acheson Process, in: Weimer, A.W. (Ed.), Carbide, Nitride and Boride Materials Synthesis and Processing. Springer Netherlands, pp. 115–129.

Gupta, G.S., Kumar, P.V., Rudolph, V.R., Gupta, M., 2001, "Heat-transfer model for the Acheson process", *Metall and Mat Trans A* 32: 1301–1308.

Hischier, R., Althaus H.-J., Bauer, Chr., Doka, G., Frischknecht R., Jungbluth N., Margni M., Nemecek, T., Simons A., Spielmann M., 2009. Documentation of changes implemented in ecoinvent Data v2.1. Dübendorf. CH.

Hodge, F. G. and L. Dominey, 2010, "Cobalt and Cobalt Alloys" *Kirk-Othmer Encyclopedia of Chemical Technology*, Hoboken, New Jersey: Wiley-Interscience.

Humbird, D., R. Davis, L. Tao, C. Kinchin, D. Hsu, A. Aden, P. Schoen, J. Lukas, B. Olthof, M. Worley, D. Sexton, and D. Dudgeon, 2011, "Process Design and Economics for Biochemical Conversion of Lignocellulosic Biomass to Ethanol," National Renewable Energy Laboratory Technical Report (NREL/TP-5100-47764), May.

Hupp, T.R., Lewis, I.C., Criscione, J.M., Reddy, R.L., Fulgenzi, C.F., Page, D.J., Fisher, F.F., Dzermejko, A.J., Hedge, J.B., 2003. Graphite, Artificial, in: Kirk-Othmer Encyclopedia of Chemical Technology. John Wiley & Sons, Inc.

Jäger, H., Frohs, W., Banek, M., Christ, M., Daimer, J., Fendt, F., Friedrich, C., Gojny, F., Hiltmann, F., Meyer zu Reckendorf, R., Montminy, J., Ostermann, H., Müller, N., Wimmer, K., von Sturm, F., Wege, E., Roussel, K., Handl, W., 2010. Carbon, 4. Industrial Carbons, in: Ullmann's Encyclopedia of Industrial Chemistry. Wiley-VCH Verlag GmbH & Co. KGaA.

Johnson, M.C., I. Palou-Rivera, and E.D. Frank, 2013, "Energy Consumption during the Manufacture of Nutrients for Algae Cultivation," *Algal Research*. doi:10.1016/j.algal.2013.08.003.

Kamienski, C.W., McDonald, D.P., Stark, M.W., Papcun, J.R., 2004. Lithium and Lithium Compounds, in: Kirk-Othmer Encyclopedia of Chemical Technology. John Wiley & Sons, Inc.

Kang, S., P. Kempgens, S. Greenbaum, A.J. Kropf, K. Amine, and M.M. Thackeray, 2006, "Interpreting the Structural and Electrochemical Complexity of $0.5Li_2MnO_3 \cdot 0.5LiMO_2$ Electrodes for Lithium Batteries (M=$Mn_{0.5-x}Ni_{0.5-x}Co_{2x}$, $0 \leq x \leq 0.5$)," *Journal of Materials Chemistry* 17: 2069–2077.

Keoleian,G., S. Miller, R. De Kleine, A. Fang, J. Mosley., 2012, "Life Cycle Material Data Update for GREET Model," Center for Sustainable Systems Report CSS12-12, available at https://greet.es.anl.gov/publication-greet2-lca-update

Laboratory, O.R.N., Enthalpy and Heat Capacity of Lithium Chloride, Potassium Chloride Eutectic. 1953.

Lee, M.-H., Y.-J. Kang, S.-T. Myung, and Y.-K. Sun, 2004, "Synthetic Optimization of Li[N$_{1/3}$Co$_{1/3}$Mn$_{1/3}$]O$_2$ via Co-precipitation,"*Electrochemica Acta* 50: 939.

Li, B., X. Gao, J. Li, and C. Yuan, 2014, "Life Cycle Environmental Impact of High-capacity Lithium Ion Battery with Silicon Nanowires Anode for Electric Vehicles," *Environmental Science and Technology*, doi:10.1021/es4037786.

LKAB (Luossavaara-Kiirunavaara Aktiebolag), 2011, *Annual Sustainability Report*.

Long, M., Sheng, J., Liu, T., Chen, D., Yang, Y., Gong, S., Chen, C., 2015. Thermo-Physical Properties of Petroleum Coke during Calcining Graphitization Process, in: Battle, T.P., Downey, J.P., D.y, L., Davis, B., Neelameggham, N.R., Sanchez-Segado, S., Pistorius, P.C. (Eds.), Drying, Roasting, and Calcining of Minerals. John Wiley & Sons, Inc., pp. 193–199.

Majeau-Bettez, G., T.R. Hawkins, and A.H. Strømman, 2011, "Life Cycle Environmental Assessment of Lithium-Ion and Nickel Metal Hydride Batteries for Plug-In Hybrid and Battery Electric Vehicles. Supporting Information," *Environmental Science and Technology* 45 (10): 4548.

Mudd, G. M. "Nickel Sulfide Versus Laterite: The Hard Sustainability Challenge Remains." *Proc. 48th Annual Conference of Metallurgists*, Canadian Metallurgical Society, Sudbury, Ontario, Canada, August 2009.

Nakumura, T., H. Sadamura, M. Hatatani, A. Kajiyama, and Y. Okuda, 2000, *Process for Producing Lithium-Cobalt Oxide*, United States Patent 6103213, August 15.

Nevada Department of Conservation and Natural Resources (NCNR), 2010, *Class II Air Quality Operating Permit*, Permit Number AP1479-0050.02, Chemetall Foote Corporation, Silver Peak, NV.

Nelson, P.A., K.G. Gallagher, I. Bloom, and D.W. Dees, 2011, "Modeling the Performance and Cost of Lithium-Ion Batteries for Electric-Drive Vehicles," Report ANL-11/32, Argonne National Laboratory, Argonne, Ill.

NETL (National Energy Technology Laboratory), 2007, "Baseline Technical and Economic Assessment of a Commercial Scale Fischer-Tropsch Liquids Facility," Report DOE/NETL-2007/1260.

Neubauer, J., and A. Pesaran, 2010, "NREL's PHEV/EV Li-Ion Battery Secondary-Use Project," presented at the Advanced Automotive Batteries Conference, Orlando, Fla., May 17–21.

NIST (National Institute of Standards and Technology), "Cobalt Oxide," *Chemistry WebBook*, Material Measurement Laboratory, http://webbook.nist.gov/cgi/cbook.cgi?ID=C1307966&Type=JANAFS&Table=on, accessed November 9, 2013.

NIST (National Institute of Standards and Technology), "Lithium", *Chemistry WebBook*, Material Measurement Laboratory, http://webbook.nist.gov/cgi/cbook.cgi?Name=lithium&Units=SI&cTG=on&cTC=on&cTP=on, accessed July 30, 2015.

Notter, D.A., M. Gauch, R. Widmer, P. Wager, A. Stamp, R. Zah, and H.-J. Althaus, 2010, "Contribution of Li-Ion Batteries to the Environmental Impact of Electric Vehicles," *Environmental Science & Technology* **44**, 6550–6556.

OrbiChem, 2013. Chem-net Facts: Chlorine. http://www.orbichem.com/userfiles/CNF%20Samples/chl_13_11.pdf, accessed July 23, 2015.

Perry, R.H., and D.W. Green (Eds.), 1997, *Perry's Chemical Engineering Handbook*, New York: McGraw Hill.

Pisarczyk, K., and Updated by Staff, 2005, "Manganese Compounds," *Kirk-Othmer Encyclopedia of Chemical Technology*, Hoboken, New Jersey: Wiley-Interscience.

Predel, H., 2014. Petroleum Coke, in: Ullmann's Encyclopedia of Industrial Chemistry. Wiley-VCH Verlag GmbH & Co. KGaA.

Richardson, H.W., 2003, "Cobalt Compounds," *Kirk-Othmer Encyclopedia of Chemical Technology*, Hoboken, New Jersey: Wiley-Interscience.

Sadoway, D.R., 1998, "Toward new technologies for the production of lithium", *Journal of the Minerals, Metals & Materials Society* 50(5): 24-26.

Schlag, S., J. Glauser, and K. Yokose, 2008, *Sodium Chloride*, CEH Product Review, SRI Consulting, Zurich, Switzerland.

Schlag, S., 2012, *Sodium Chlorate*, CEH Product Review, SRI Consulting, Zurich, Switzerland.

Shaw, S., 2013. Graphite demand growth: the future of lithium-ion batteries in EVs and HEVs. http://www.roskill.com/reports/industrial-minerals/news/download-roskills-paper-on-graphite-demand-growth-the-future-of-lithium-ion-batteries-in-evs-and-hevs/at_download/attachment1, accessed June 9, 2015.

Spitzer, J.J., P.P. Sing, K.G. McCurdy, and L.G. Hepler, 1978, "Apparent Molar Heat Capacities and Volumes of Aqueous Electrolytes: $CaCl_2$, $Cd(NO_3)_2$, $CoCl_2$, $Cu(ClO_4)_2$, $Mg(ClO_4)_2$, $NiCl_2$," *Journal of Solution Chemistry* 7: 81–86.

Stamp, A., Lang, D.J., Wäger, P.A., 2012, "Environmental impacts of a transition toward e-mobility: the present and future role of lithium carbonate production", *Journal of Cleaner Production* 23: 104–112.

Stolzenberg, A.M., 2004, "Iron Compounds," *Kirk-Othmer Encyclopedia of Chemical Technology*, Hoboken, New Jersey: Wiley-Interscience.

Tamashausky, A.V., 2006. An Introduction to Synthetic Graphite: http://asbury.com/pdf/SyntheticGraphitePartI.pdf, accessed May 29, 2015.

Thackeray, M.M., S. Kang, C.S. Johnson, J.T. Vaughye, R. Benedek, and S.A. Hackney, 2007 , "Li_2MnO_3-Stabilized $LiMO_2$ (M = Mn, Ni, Co) Electrodes for Lithium-ion Batteries," *Journal of Materials Chemistry* 17: 3112–3125.

Tundermann, J.H., J.K. Tien, T.E. Howson, and Updated by Staff, 2013, "Nickel and Nickel Alloys," *Kirk-Othmer Encyclopedia of Chemical Technology*, Hoboken, New Jersey: Wiley-Interscience.

The Aluminum Association. 2013. The Environmental footprint of semi-finished aluminum products in North America. http://www.aluminum.org/sites/default/files/LCA_Report_Aluminum_Association_12_13.pdf

The Gold Report, 2014. Tesla Gigafactory Could Be Boon for Graphite, Lithium, Cobalt: Simon Moores. http://www.theaureport.com/pub/na/tesla-gigafactory-could-be-boon-for-graphite-lithium-cobalt-simon-moores, accessed May 26, 2015.

University of Minnesota, 2011, Minnesota Technical Assistance Program: Energy efficiency opportunities for metal casters. http://www.mntap.umn.edu/metalcast/energy.htm, accessed June 20, 2015.

U.S. Department of Energy. 1999. Energy and environmental profile of the U.S. metalcasting industry. http://energy.gov/sites/prod/files/2013/11/f4/profile_0.pdf

USGS 2013a. Minerals Yearbook: Lithium http://minerals.usgs.gov/minerals/pubs/commodity/lithium/myb1-2013-lithi.pdf

USGS 2013b. Metal Prices in the United States through 2010. http://pubs.usgs.gov/sir/2012/5188/

USGS 2012 Minerals Yearbook: Graphite http://minerals.usgs.gov/minerals/pubs/commodity/graphite/myb1-2012-graph.pdf

Wang, H., Yang, Y., Liang, Y., Robinson, J.T., Li, Y., Jackson, A., Cui, Y., Dai, H., 2011, "Graphene-Wrapped Sulfur Particles as a Rechargeable Lithium–Sulfur Battery Cathode Material with High Capacity and Cycling Stability", *Nano Lett.* 11: 2644–2647.

Wang, Q.Y., J. Liu, V. Murugan, and A. Manthiram, 2009, "High Capacity Double-layer Surface Modified Li[Li$_{0.2}$Mn$_{0.54}$Ni$_{0.13}$Co$_{0.13}$]O$_2$ Cathode with Improved Rate Capability," *Journal of Materials Chemistry* 19: 4965–4972.

Wietelmann, U., Steinbild, M., 2014. Lithium and Lithium Compounds, in: Ullmann's Encyclopedia of Industrial Chemistry. Wiley-VCH Verlag GmbH & Co. KGaA.

Wilcox, J.D., M.M. Doeff, M. Marcinek, and R. Kostecki, 2007, "Factors Influencing the Quality of Carbon Coatings on LiFePO$_4$," *Journal of the Electrochemical Society* 154 (5): A389.

Yoshino, A., 2014. 1 - Development of the Lithium-Ion Battery and Recent Technological Trends, in: Pistoia, G. (Ed.), Lithium-Ion Batteries. Elsevier, Amsterdam, pp. 1–20.

Yu, J.G., Li, B., Li, S.Z., Lou, J.W., Shen, M., 2011. Method for removing impurity MgCl2 from lithium electrolyte KCl-LiCl. Chinese Patent 102002730 A, April 6.

APPENDIX A   MASS INVENTORY SUMMARY

Tables A-1 through A-4 in this appendix summarize BatPaC results for the compositions of hybrid electric vehicle (HEV), plug-in HEV (PHEV), and battery EV (BEV) batteries with different cathode materials. The lithium and manganese-rich metal oxide $0.5Li_2MnO_3 \cdot 0.5LiNi_{0.44}Co_{0.25}Mn_{0.31}O_2$ (LMR-NMC) and lithium cobalt oxide ($LiCoO_2$, or LCO) are provided as cathode options only for BEV batteries because they are used primarily in high-energy applications. The sums of reported weight percentages may not total to 100% because of rounding.

Table A-1   Mass Inventory for Varying Cathode Materials for the HEV

Material (wt%)	LFP[a]	NMC	LMO[b]
Active Material	17	16	25
Wrought Aluminum	22	23	20
Copper	15	19	12
Graphite/Carbon	11	10	11
Electrolyte: Ethylene Carbonate	5.7	4.0	4.1
Electrolyte: Dimethyl Carbonate	5.7	4.0	4.1
Electrolyte: $LiPF_6$	2.0	1.4	1.4
Electronic Parts	10	10	11
Steel	3.5	3.3	3.3
Binder	1.4	1.4	1.9
Polypropylene	2.3	2.8	1.8
Polyethylene	0.35	0.48	0.23
Polyethylene Terephthalate	2.2	2.0	2.0
Glycol (coolant)	1.9	1.8	1.9
Thermal Insulation	0.36	0.34	0.36
Total Mass (kg)	24	23	21

[a]   LFP = lithium iron phosphate ($LiFePO_4$).

[b]   LMO = lithium manganese oxide.

Table A-2   Mass Inventory for Varying Cathode Materials for PHEVs

Material (wt%)	Split PHEV			Series PHEV		
	LFP	NMC	LMO	LFP	NMC	LMO
Active Material	22	24	30	17	15	27
Wrought Aluminum	23	22	21	27	26	22
Copper	12	13	11	19	25	15
Graphite/Carbon	14	16	13	11	9.7	12
Electrolyte: Ethylene Carbonate	6.9	4.8	4.8	6.3	4.7	4.8
Electrolyte: Dimethyl Carbonate	6.9	4.8	4.8	6.3	4.7	4.8
Electrolyte: $LiPF_6$	2.4	1.7	1.7	2.2	1.6	1.7
Electronic Parts	2.8	3.5	3.1	2.2	2.2	2.8
Steel	2.2	2.0	2.0	2.1	2.0	2.0
Binder	1.9	2.1	2.3	1.4	1.3	2.1
Polypropylene	2.0	2.0	1.8	2.9	3.7	2.2
Polyethylene	0.30	0.32	0.26	0.52	0.75	0.38
Polyethylene Terephthalate	1.9	1.7	1.7	1.8	1.6	1.7
Glycol (coolant)	2.0	2.3	1.7	1.2	1.1	1.3
Thermal Insulation	0.36	0.37	0.35	0.42	0.30	0.34
Total Mass (kg)	84	68	76	107	108	85

Table A-3   Mass Inventory for Varying Cathode Materials in EV Batteries

Material (wt%)	80 kW				115 kW				149 kW			
	LFP	NMC	LCO	LMO	LFP	NMC	LCO	LMO	LFP	NMC	LCO	LMO
Active Material	24	30.	29	34	24	30.	29	34	24	28	29	34
Wrought Aluminum	20.	19	19	19	20.	19	19	19	20.	20.	20.	19
Copper	13	10.	10.	11	12	9.7	9.8	11	12	11	11	11
Graphite/Carbon	15	20.	19	15	15	19	19	15	15	18	18	15
Electrolyte: Ethylene Carbonate	7.7	5.4	5.4	5.4	7.8	5.4	5.4	5.4	7.8	5.4	5.4	5.4
Electrolyte: Dimethyl Carbonate	7.8	5.4	5.4	5.4	7.8	5.4	5.4	5.4	7.8	5.4	5.4	5.4
Electrolyte: $LiPF_6$	2.7	1.9	1.9	1.9	2.7	1.9	1.9	1.9	2.7	1.9	1.9	1.9
Electronic Parts	1.0	1.4	1.4	1.1	1.0	1.4	1.4	0.33	1.0	1.3	1.4	1.1
Steel	1.6	1.4	1.4	1.4	1.6	1.4	1.4	1.4	1.6	1.4	1.4	1.4
Binder	2.1	2.6	2.6	2.5	2.1	2.6	2.6	2.6	2.1	2.5	2.5	2.5
Polypropylene	1.9	1.5	1.5	1.7	1.9	1.5	1.5	1.7	1.9	1.7	1.6	1.7
Polyethylene	0.33	0.24	0.24	0.29	0.33	0.24	0.24	0.29	0.33	0.30	0.28	0.29
Polyethylene Terephthalate	1.4	1.2	1.2	1.2	1.4	1.2	1.2	1.2	1.4	1.2	1.2	1.2
Glycol (coolant)	0.9	1.1	1.1	0.95	0.99	1.1	1.1	0.95	0.99	1.0	1.1	0.95
Thermal Insulation	0.35	0.37	0.37	0.33	0.35	0.37	0.37	0.33	0.35	0.36	0.37	0.33
Total Mass (kg)	230	170	160	210	230	170	160	210	230	180	170	210

Table A-4 Mass Inventory for Varying Anode Materials (with LMR-NMC as the Cathode) for EVs

Material (wt%)	80 kW		115 kW		135+ kW	
	G[a]	Gr-Si[b]	G	Gr-Si	G	Gr-Si
Active Material	21	29	21	26	20.	24
Wrought Aluminum	21	23	22	24	22	25
Copper	12	14	13	18	15	20.
Graphite/Carbon	22	6.8	22	6.0	20.	5.6
Electrolyte: Ethylene Carbonate	5.6	5.8	5.6	5.6	5.5	5.6
Electrolyte: Dimethyl Carbonate	5.6	5.8	5.6	5.6	5.5	5.6
Electrolyte: $LiPF_6$	1.9	2.0	1.9	1.9	1.9	1.9
Electronic Parts	1.6	2.0	1.6	1.8	1.5	1.7
Steel	1.4	1.3	1.4	1.3	1.4	1.2
Binder	2.3	2.5	2.2	2.2	2.1	2.1
Polypropylene	1.7	2.0	1.8	2.5	2.1	2.8
Polyethylene	0.29	0.37	0.33	0.50	0.40	0.56
Polyethylene Terephthalate	1.2	1.2	1.2	1.2	1.2	1.2
Glycol (coolant)	1.3	1.8	1.3	1.4	1.1	1.3
Thermal Insulation	0.41	0.45	0.40	0.42	0.39	0.41
Total Mass (kg)	150	120	150	130	160	140

[a] G = graphite.

[b] Gr-Si = graphite silicon.